to appear in: Dynamical Systems and Applications

Burst and spike synchronization of coupled neural oscillators

Jürgen Schwarz[1,3], Gerhard Dangelmayr[2], Andreas Stevens[3], and Kurt Bräuer[1]

[1]Institut für Theoretische Physik, Universität Tübingen,
Morgenstelle 14, D-72076 Tübingen, Germany

[2]Departement of Mathematics, Colorado State University,
121 Engineering Building, Ft. Collins, CO 80523, USA

[3]Universitätsklinik für Psychiatrie und Psychotherapie,
Osianderstr. 24, D-72076 Tübingen, Germany

submitted: 11/19/1999; revised: 12/01/2000

Abstract

Neural excitability and the bifurcations involved in transitions from quiescence to oscillations largely determine the neuro-computational properties of neurons. Neurons near Hopf bifurcation fire in a small frequency range, respond preferentially to resonant excitation, and are easily synchronized. In the present paper we study the interaction of coupled elliptic bursters with non-resonant spike frequencies. Bursting behavior arises from recurrent transitions between a quiescent state and repetitive firing, i.e., the rapid oscillatory behavior is modulated by a slowly varying dynamical process. Bursting is referred to as elliptic bursting when the rest state loses stability via a Hopf bifurcation and the repetitive firing disappears via another Hopf bifurcation or a double limit cycle bifurcation. By studying the fast subsystem of two coupled bursters we obtain a reduced system of equations, allowing the description of synchronized and non-synchronized oscillations depending on frequency detuning and mutual coupling strength. We show that a certain "overall" coupling constant must exceed a critical value depending on the detuning and the attraction rates in order that burst and spike synchronization can take place. The reduced systen allows an analytical study of the bifurcation structure up to codimension-3 revealing a variety of stationary and periodic bifurcations which will be analyzed in detail. Finally, the implications of the bifurcation structure for burst and spike synchronization are discussed.

corresponding author:
Jürgen Schwarz
Institut für Theoretische Physik, Morgenstelle 14, D-72076 Tübingen, Germany
Tel: ++49 7071 29 76377
Fax: ++49 7071 29 5604
email: juergen.schwarz@uni-tuebingen.de,

1 Introduction

The dynamic mechanisms of the generation of action potentials and the transitions from quiescent to periodic activity are of particular importance in understanding communication and signaling between neurons. Action potentials are generated by ionic currents through the cell membrane and may arise due to intracellular mechanisms destabilizing the steady state or as a response to external stimulation. The neuron is said to be excitable if a small perturbation of the rest state results in a large excursion of the potential – a spike. According to their response on external stimulation, Hodgkin (1948) suggested to distinguish at least two different classes of neural excitability. The qualitative distinction is that the emerging oscillations of so-called class-1 neurons have fixed amplitude and an arbitrarily small frequency, whereas class-2 neurons initiate firing with nonzero frequency and a small amplitude. The class of neural excitability is closely related to the bifurcation resulting in transition from rest to repetitive firing (Ermentrout, 1996; Hoppensteadt and Izhikevich, 1997). If we consider codimension-1 bifurcations involving fixed points that give rise to oscillations then class-1 excitability corresponds to a saddle node on circle (or limit cycle) bifurcation and class-2 excitability corresponds to a Hopf bifurcation. The different types of bifurcations determine the neuro-computational properties of neurons. A class-1 neuron can fire with arbitrarily low frequency and it acts as an integrator, i.e., the higher the input frequency the sooner it fires. A class-2 neuron fires in a certain, small frequency range and it acts as a resonator, i.e., it responds preferentially to resonant input (Hoppensteadt and Izhikevich, 1997).

When the dynamics alternates between rest and repetitive spiking the firing pattern is called bursting. Bursting requires a dynamics on two different time scales, where the transition from quiescent to repetitive spiking activity is governed by fast membrane voltage dynamics and the firing is modulated by slow voltage-dependent processes. Models of bursting introduce an additional dynamical variable and can be written in the singularly perturbed form

$$\begin{aligned} \dot{x} &= f(x,y) \\ \dot{y} &= \mu g(x,y), \end{aligned} \tag{1}$$

where x, y describes the fast/slow dynamics, and $\mu \ll 1$ is the ratio of fast/slow time scales (Bertram et al., 1995; Wang and Rinzel, 1995; Izhikevich, 2000a). The silent phase corresponds to x being at the steady state and the active phase to x being on a limit cycle. Since for generation and termination of bursting at least two bifurcations are involved (one for rest/oscillatory and one for oscillatory/rest transition) there are many different types of bursters [for review and full classification of planar bursters see Izhikevich (2000a)]. Bursting is referred to as elliptic bursting when the rest state loses stability via Hopf bifurcation and the repetitive firing may disappear via another Hopf bifurcation or a double limit cycle bifurcation (on which a pair of stable/unstable limit cycles coalesce and vanish). Since Hopf and double limit cycle bifurcation may be subcritical or supercritical there are several subtypes of elliptic bursting. Analysis of models of bursting is accomplished by examining the bifurcation structure of the fast subsystem, treating the slow variables y as quasi-static bifurcation parameters u of the system $\dot{x} = f(x, u)$. To consider the dynamics of x and y separately is known as dissection of neural bursting (Rinzel and Lee, 1987).

A general theory of weakly connected neural models was developed by Hoppensteadt and Izhikevich (1997). It supposes the idea that the dynamics of each neuron is near a bifurcation which allows weak interactions between similar neurons. This enables to study high-dimensional neurons by using simpler low-dimensional dynamical systems by so-called canonical models. Briefly, a model is canonical for a family of dynamical systems if every member of the family can be transformed by a piece-wise continuous, possibly non-invertible, change of variables into the canonical model. The advantage of a canonical model is its universality since it provides information on the behavior of the entire family. The canonical model for local subcritical elliptic bursting was proposed by Izhikevich (2000b). It has the form

$$\dot{z} = (u + i\Omega)z + \sigma z|z|^2 + \rho z|z|^4 \,, \tag{2a}$$
$$\dot{u} = \mu(a - |z|^2) \,, \tag{2b}$$

where $z \in \mathbb{C}$ and $u \in \mathbb{R}$ are the fast and slow variables, Ω is the fequency, a, μ are real parameters with $\mu \ll 1$ and σ, ρ may in general be complex with $\sigma_r = \mathrm{Re}(\sigma) > 0$, $\rho_r = \mathrm{Re}(\rho) < 0$. The model is canonical since the fast subsystem (2a) is derived via normal form transformation of an arbitrary system of the form (1). It is well known that the fifth-order normal form for a Hopf bifurcation exhibits Hopf and double limit cycle bifurcation. The codimension-2 point in the parameter space where both bifurcation sets meet tangentially is referred to as degenerate Hopf or Bautin bifurcation point. Bursting occurs due to the dynamics of the slow subsystem (2b) which crosses the bifurcation curves for Hopf bifurcation (u=0) and double limit cycle bifurcation ($u = \sigma_r^2/4\rho_r$) periodically.

The behavior of (2a), (2b) can be examined as follows. Let $r = |z|$ denote the amplitude of oscillation of the fast variable z and rewrite the radial part of (2a) and (2b) in the form

$$\begin{aligned} \dot{r} &= ur + \sigma_r r^3 + \rho_r r^5 \,, \\ \dot{u} &= \mu(a - r^2) \,. \end{aligned} \tag{3}$$

The system (3) has a unique equilibrium $(r, u) = \left(\sqrt{a}, -\rho_r a^2 - \sigma_r a\right)$ for all μ and $a > 0$, which is stable when $a > -2\sigma_r/\rho_r$. For $0 < a < -\sigma_r/2\rho_r$ the system (3) has a slow limit cycle attractor resulting in bursting behavior of the full system (2a), (2b) which is is depicted in Figure 1. The parameter a determines the length of the interburst period and for a close to the Hopf bifurcation of (3) at $a = -2\sigma_r/\rho_r$ the bursting looks like periodic (tonic) spiking.

A first study of synchronization of coupled elliptic bursters was given by Izhikevich (2000a; 2000b) for the case that both bursters are identical. Since there are two rhythmic processes associated with each burster, viz. repetitive spiking and repetitive bursting, there could be at least two different regimes of synchronization: synchronization of individual spikes and synchronization of bursts. The main finding was that spike synchronization within a single burst crucially depends on the interspike frequency and in general is difficult to achieve. Elliptic bursters do not interact unless they have matching interspike frequencies. For bursters with equal frequencies one can then show that the spike firing synchronizes, i.e., the activity of the fast subsystem converges to a limit cycle (Izhikevich, 2000b). Burst synchronization is difficult to avoid and is mediated by two mechanisms. First, at onset of bursting, a delay of the transition between the stable steady state and oscillations can occur when the control parameter slowly passes through the Hopf bifurcation point, which is referred to as slow passage effect (Baer et al., 1989). The passage can be shortened significantly by weak input or noise from other bursters (Izhikevich, 2000b). Second, at termination of bursting, any differences between the slow variables u_i diminish rapidly, which is referred to as fast threshold modulation and can be observed in strongly coupled relaxation oscillators (Somers and Kopell, 1993; Izhikevich, 2000a).

The restriction to weak coupling is biologically plausible and discussed in detail by Hoppensteadt and Izhikevich (1997). On the other hand, there is also ample experimental evidence that variations

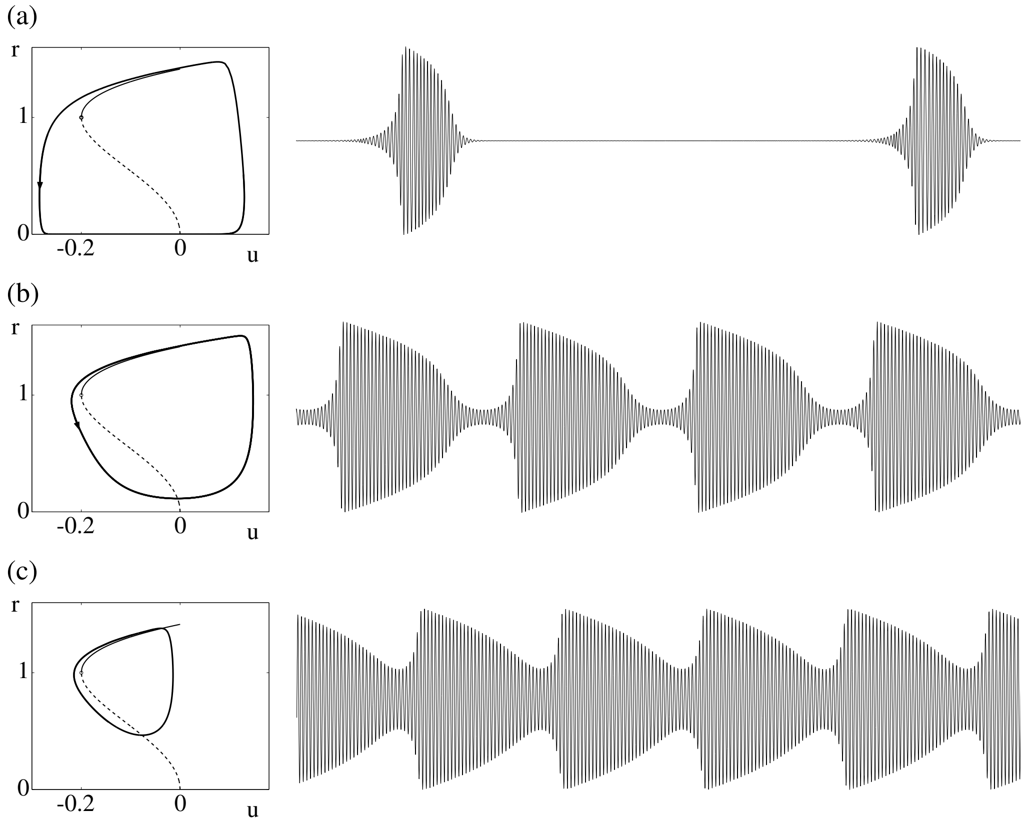

Figure 1: Simulations of (2a), (2b) for $\Omega = 3$, $\sigma = 0.4$, $\rho = -0.2$, $\mu = 0.01$ showing elliptic bursting for (a) $a = .1$, (b) $a = .9$, (c) $a = .96$ (close to the Hopf bifurcation at $a = 1$ of the (r, u)-system). The left graphs show the nullclines and the phase portraits according to (3). On the right the corresponding bursting patterns of the variable $y = \mathrm{Im}(z)$ are shown.

in synaptic coupling may modify the neuro-computational properties of neurons (Liljenström and Hasselmo, 1995; Gil et al., 1997), or that strong coupling may lead to instabilities that give rise to physiologically significant bifurcations (Bressloff and Coombes, 1998). Experimental estimates of coupling strength are difficult to achieve and may vary between different regions in the brain. Individual neurons may be weakly connected, however, the coupling between neural populations or the coupling strength of external input to the system might not be. Generally, the strength of connections between neurons depends on the current state of neurotransmitter and neuromodulator release and varies with the temporal activity in the network.

In this paper we study two coupled elliptic bursters to see how synaptic coupling strength and frequency mismatch affects synchronization. For simplicity we assume that both bursters are identical except for their center frequencies Ω_i. We also assume that only the fast subsystems are interconnected, which is justified since synaptic transmission is mainly triggered by fast ion channels, and that the coupling involves only the imaginary parts. As shown by Izhikevich (2000b) other synaptic configurations, such as connections between the fast and slow subsystems, or between the slow subsystems, can be removed by an appropriate continuous change of variables. With these assumptions and suitable normalizations of σ_r, ρ_r the equations for two coupled elliptic bursters take the form

$$\begin{aligned}\dot{z}_1 &= (u_1 + i\Omega_1)z_1 + (\frac{2}{5} + ip)|z_1|^2 z_1 - (\frac{1}{5} - iq)|z_1|^4 z_1 + \frac{k}{2}(z_2 - \bar{z}_2)\,, \\ \dot{z}_2 &= (u_2 + i\Omega_2)z_2 + (\frac{2}{5} + ip)|z_2|^2 z_2 - (\frac{1}{5} - iq)|z_2|^4 z_2 + \frac{k}{2}(z_1 - \bar{z}_1)\,,\end{aligned} \tag{4a}$$

and

$$\begin{aligned}\dot{u}_1 &= \mu(a - |z_1|^2)\,, \\ \dot{u}_2 &= \mu(a - |z_2|^2)\,.\end{aligned} \tag{4b}$$

We refer to (4a) with u_1, u_2 considered as parameters ($\mu = 0$ in (4b)) as the fast subsystem. This system consists of two coupled Hopf-type oscillators and depends on three basic parameters k, u_1, u_2. Understanding the bifurcations of (4a) in dependence of these parameters is of high importance for understanding the dynamics of the full system (4a),(4b), since sections $k = \text{const}$ of the bifurcation set play the role of slow manifolds of the full system.

In the next section we consider first a more general class of coupled Hopf-type oscillators and derive and analyze phase equations assuming small detuning and couplings. When specified to (4a), this allows us to discriminate between phase locking and non-synchronized oscillations in dependence of k and to determine the corresponding frequencies and averaged frequencies, respectively. In Section 3 we present results of a bifurcation analysis of (4a) for $u_1 = u_2$. In order to make this study accessible to analytic computations we make the simplifying assumption $p = q = 0$. A consequence of this assumption is that we can distinguish "symmetric" and "non-symmetric" solutions which greatly simplifies the analysis and helps to organize the bifurcations. In Section 4 we give a qualitative description of the implications of our bifurcation analysis for the full system (4a),(4b). The results are summarized and discussed further in the concluding Section 5.

2 Phase equations

Consider two general, linearly coupled Hopf-type oscillators of the form

$$\dot{z}_i = f_i(|z_i|^2)z_i + (k_{i1} + ik_{i2})z_j + (k_{i3} + ik_{i4})\bar{z}_j\,, \tag{5}$$

where $(i,j) = (1,2)$ and $(i,j) = (2,1)$. Here, f_1, f_2 are smooth complex valued functions describing the individual oscillators and the k_{ij} are real coupling constants. Transformed into polar coordinates, $z_i = r_i \exp(i\varphi_i)$, (5) takes the form

$$\begin{aligned}\dot{r}_1 &= f_{1r}(r_1) + r_2\big(k_{11}\cos\phi + k_{12}\sin\phi + k_{13}\cos 2\Phi + k_{14}\sin 2\Phi\big) \\ \dot{r}_2 &= f_{2r}(r_2) + r_1\big(k_{21}\cos\phi - k_{22}\sin\phi + k_{23}\cos 2\Phi + k_{24}\sin 2\Phi\big)\end{aligned} \tag{6a}$$

$$\begin{aligned}\dot{\varphi}_1 &= f_{1\varphi}(r_1) + \frac{r_2}{r_1}\big(k_{12}\cos\phi - k_{11}\sin\phi + k_{14}\cos 2\Phi - k_{13}\sin 2\Phi\big) \\ \dot{\varphi}_2 &= f_{2\varphi}(r_2) + \frac{r_1}{r_2}\big(k_{22}\cos\phi + k_{21}\sin\phi + k_{24}\cos 2\Phi - k_{23}\sin 2\Phi\big)\end{aligned} \tag{6b}$$

where $f_{ir}(r_i) = Re[r_i f_i(r_i^2)]$, $f_{i\varphi}(r_i) = Im[f_i(r_i^2)]$, and ϕ and Φ are the phase difference and average phase, respectively,

$$\phi = \varphi_1 - \varphi_2, \;\; \Phi = \frac{1}{2}(\varphi_1 + \varphi_2).$$

If we assume that the uncoupled oscillators show stable limit cycles with fixed radii $r_i = r_{is}$, i.e., $f_{ir}(r_{is}) = 0$, and frequencies $\dot{\varphi}_i = f_{i\varphi}(r_{is}) \equiv \omega_{is}$, and if the coupling constants are sufficiently small, there exists an invariant torus for (5) on which the radii are functions of (ϕ, Φ). Defining

$$\Delta = \omega_{1s} - \omega_{2s}, \;\; \bar{\omega} = \frac{1}{2}(\omega_{1s} + \omega_{2s}),$$

and assuming that Δ also is sufficiently small, a perturbation calculation based on the invariance condition leads, up to linear order in Δ and the coupling constants, to the following dependence of the radii on the phases on the torus,

$$\begin{aligned} r_1 &= r_{1s} - \frac{r_{2s}}{\Gamma_1}\big(k_{11}\cos\phi + k_{12}\sin\phi\big) + C_1\cos 2\Phi + D_1 \sin 2\Phi\,, \\ r_2 &= r_{2s} - \frac{r_{1s}}{\Gamma_2}\big(k_{21}\cos\phi - k_{22}\sin\phi\big) + C_2\cos 2\Phi + D_2 \sin 2\Phi\,. \end{aligned} \tag{7}$$

In (7), $\Gamma_i = df_{ir}/dr_i|_{r_{is}}$, $(i = 1, 2)$, are the attraction rates of the individual limit cycles in the absence of couplings, and C_i, D_i are further coefficients which are not needed explicitely. By substituting (7) into (6b) and averaging over Φ (which is justified if $|\Delta| \ll |\bar{\omega}|$), we obtain

$$\dot{\varphi}_i = \omega_{is} + \kappa_{i1}\cos\phi + \kappa_{i2}\sin\phi \;\; (i = 1, 2), \tag{8}$$

where

$$\kappa_{i1} = r_{js}\Big(\frac{k_{i2}}{r_{is}} - \frac{k_{i1}\sigma_i}{\Gamma_i}\Big), \;\; \kappa_{i2} = (-1)^i r_{js}\Big(\frac{k_{i1}}{r_{is}} - \frac{k_{i2}\sigma_i}{\Gamma_i}\Big)$$

and $\sigma_i = df_{i\varphi}/dr_i|_{r_{is}}$. Thus the averaged evolution of ϕ on the invariant torus is determined by

$$\dot{\phi} = \Delta + (\kappa_{11} - \kappa_{21})\cos\phi + (\kappa_{12} - \kappa_{22})\sin\phi\,. \tag{9}$$

Defining the "overall" coupling constant k_0 and the phase ϕ_0 by

$$\kappa_{11} - \kappa_{21} = k_0 \sin\phi_0, \;\; \kappa_{12} - \kappa_{22} = -k_0\cos\phi_0,$$

i.e., $\dot{\phi} = \Delta - k_0\sin(\phi - \phi_0)$, the phase equation (9) tells that synchronization occurs if $k_0^2 > \Delta^2$. The synchronized oscillation corresponds to the stable fixed point $\phi = \phi_s$ of (9), determined by

$$\phi_s - \phi_0 = \sin^{-1}(\frac{\Delta}{k}) \tag{10}$$

and restricted to $-\pi/2 < \phi_s - \phi_0 < \pi/2$ (the solution to (10) in the complementary range is unstable). From (8) we then find that the common frequency $\dot{\varphi}_1 = \dot{\varphi}_2 \equiv \omega$ of the stable, synchronized oscillation is given by

$$\omega = \bar{\omega} + \frac{1}{2}k_1\cos(\phi_s - \phi_1)\,, \tag{11}$$

where k_1 and ϕ_1 are defined by

$$\kappa_{11} + \kappa_{21} = k_1\cos\phi_1, \;\; \kappa_{12} + \kappa_{22} = k_1 \sin\phi_1.$$

For $k_0^2 < \Delta^2$, ϕ rotates around its circle with period $T = 2\pi/\sqrt{\Delta^2 - k_0^2}$, thus there is no phase locking. In this desynchronized range we find a quasiperiodic motion on an attractive invariant torus. The dynamics on the torus can be characterized by averaged frequencies $\bar{\omega}_i$, defined by

$$\bar{\omega}_i \equiv \frac{1}{T}\int_0^T \dot{\varphi}_i dt = \omega_{is} - \frac{\Delta}{k_0}[1 - \sqrt{1 - k_0^2/\Delta^2}](\kappa_{i1}\sin\phi_0 + \kappa_{i2}\cos\phi_0)\,. \tag{12}$$

We now specify these general results to the system (4a) for which $k_{i1} = -k_{i3} = k/2$ and $k_{ij} = 0$ otherwise. Setting $u_1 = u_2 = u$, the radii $r_{1s}^2 = r_{2s}^2 \equiv r_s^2$ of the stable limit cycles and the associated attraction rates $\Gamma_1 = \Gamma_2 \equiv \Gamma$ of the uncoupled system ($k = 0$) are given by

$$r_s^2 = 1 + \sqrt{1 + 5u}, \quad \Gamma = -\frac{4r_s^2}{5}\sqrt{1 + 5u},$$

with frequencies $\omega_{is} = \Omega_i + pr_s^2 + qr_s^4$ and $\sigma_i = 2r_s(p + 2qr_s^2)$. The κ_{ij} then reduce to $\kappa_{i1} = -gk/2$, $\kappa_{i2} = k/2$ ($i = 1, 2$), where

$$g = -\frac{5p + 10qr_s^2}{2\sqrt{1 + 5u}}.$$

From this we find $k_0 = k$ and, assuming $k > 0$, that $\phi_0 = \phi_1 = 0$, hence

$$\dot{\phi} = \Delta - k\sin\phi\,. \tag{13}$$

The frequency (11) of the phase-locked state simplifies to

$$\omega = \Delta - \frac{g}{2}\sqrt{k^2 - \Delta^2}, \tag{14}$$

and the averaged frequencies (12) of the non-synchronized state become

$$\bar{\omega}_i = \omega_{is} - \frac{(-1)^i}{2}\Delta[1 - \sqrt{1 - k^2/\Delta^2}]. \tag{15}$$

Thus the main implication of the phase description of (4a) is that for k above the critical coupling $k_c = \Delta$ the oscillators are phase-locked and oscillate with the same frequency given by (14), whereas below k_c they are desynchronized and show different averaged frequencies (15).

3 Bifurcations

Besides synchronization and desynchronization, a system of two coupled oscillators may encounter a variety of further instabilities and bifurcations, see, e.g., Aronson et al. (1990) for a study of coupled third-order Hopf oscillators. Weak coupling yields a phase model and the phase description is justified if the attraction rate is strong compared to coupling strength. However, if the attraction to the limit cycle is small, amplitude effects cannot be neglected. As an example consider phenomena such as oscillator death (Bar-Eli effect) or coupling-induced spontaneous activity (self-ignition). Recall that oscillator death in coupled third-order Hopf oscillators can only occur with diffusive coupling. There the phase drift solution collapses in a Hopf bifurcation that leaves the steady state solution stable. Coupled oscillators near a Bautin bifurcation already exhibit a stable steady state and a stable/unstable pair of limit cycles simultaneously. Thus in the bistable region the limit

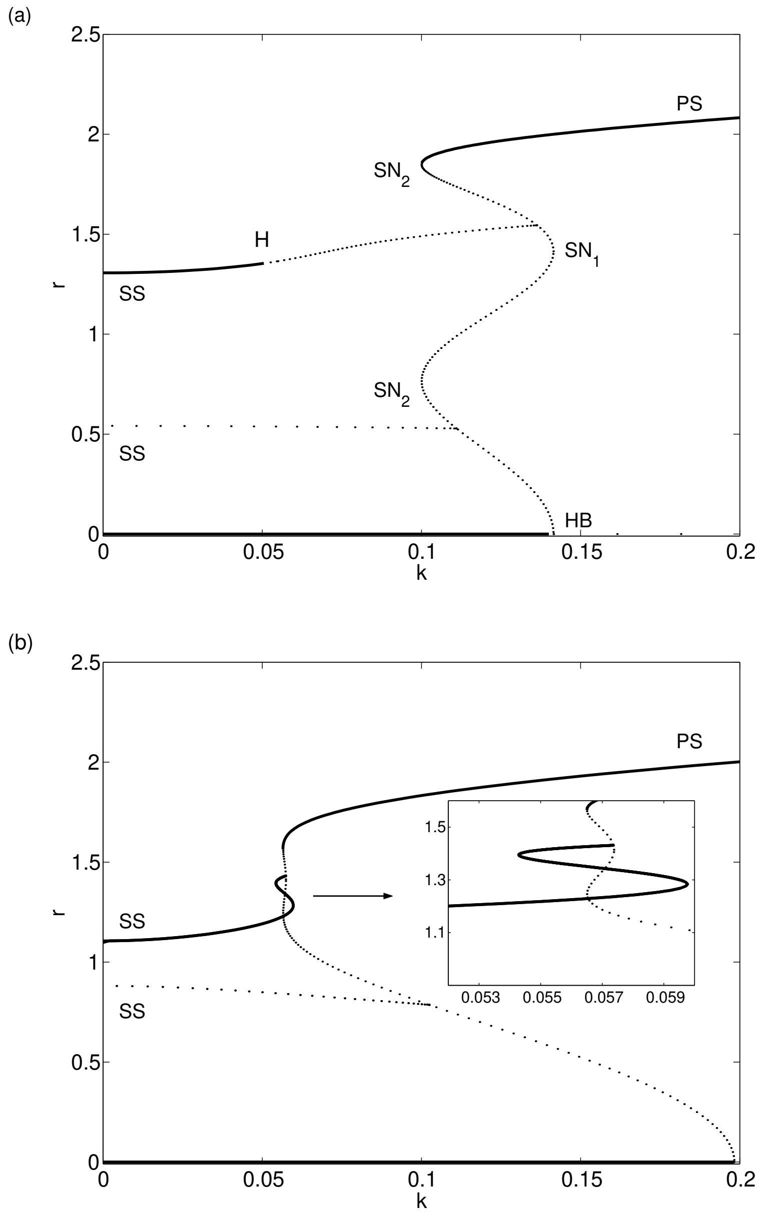

Figure 2: Bifurcation diagram of (4a) for (a) $\Omega_1 - \Omega_2 = .2$, $u = -0.1$, (b) $\Omega_1 - \Omega_2 = .113$, $u = -0.19$, $p = q = 0$ computed with the continuation package AUTO. Shown are the total amplitudes of stable (solid) and unstable (dashed) limit cycles versus coupling strength k. On the limit cycle bifurcating from the trivial solution $z_1 = z_2 = 0$ at HB both oscillators have equal amplitudes. On the two branches continued from $k = 0$ the oscillators have different amplitudes.

cycles may undergo a saddle node bifurcation where the stable and unstable limit cycles coalesces and vanishes. In this regime amplitude effects become important.

Two bifurcation diagrams of (4a) computed with the continuation package AUTO are shown in Figure 2. They show the steady state solution $r = 0$ and the limit cycle solutions for different values of detuning $\Delta = \Omega_1 - \Omega_2$ and bifurcation parameter u as functions of the coupling strength k. Several important bifurcation points can be observed. First, the stable steady state solution $r = 0$ undergoes a Hopf bifurcation (HB). On the emerging limit cycle solution both oscillators have equal amplitudes. Along this branch we can observe saddle node bifurcations labeled by SN_1 and SN_2. The single oscillator for $k = 0$ exhibits a stable and an unstable limit cycle. These solutions correspond to the two branches continued from $k = 0$. Here the oscillators have different amplitudes. For certain choices of the parameter a secondary Hopf or torus bifurcation T_S can be observed. In the following we study such types of bifurcation diagrams analytically.

3.1 Bifurcation of the steady state at zero

First we look at the trivial solution $z_1 = z_2 = 0$. Writing the characteristic equation for an eigenvalue λ of the Jacobian as

$$\lambda^4 + a_3\lambda^3 + a_2\lambda^2 + a_1\lambda + a_0 = 0,$$

the condition for a Hopf bifurcation, $\lambda = i\omega$, is given by

$$a_1^2 - a_1 a_2 a_3 + a_0 a_3^2 = 0,$$

with corresponding frequency $\omega^2 = a_1/a_3 > 0$. The coefficients of the characteristic polynomial are calculated as

$$\begin{aligned}
a_3 &= -2(u_1 + u_2)\,, \\
a_2 &= u_1^2 + u_2^2 + 4u_1u_2 + \Omega_1^2 + \Omega_2^2 - k^2\,, \\
a_1 &= (k^2 - 2u_1u_2)(u_1 + u_2) - 2u_2\Omega_1^2 - 2u_1\Omega_2^2\,, \\
a_0 &= (u_1^2 + \Omega_1^2)(u_2^2 + \Omega_2^2) - k^2u_1u_2.
\end{aligned}$$

To analyze the condition for a Hopf bifurcation we introduce average and detuning parameters

$$\Omega = \frac{1}{2}(\Omega_1 + \Omega_2),\;\; \Delta = \Omega_1 - \Omega_2,\;\; u = \frac{1}{2}(u_1 + u_2),\;\; v = u_1 - u_2, \tag{16}$$

and assume that Ω is $O(1)$ whereas Δ and k are treated as small parameters. Note that the small coupling limit excludes stationary bifurcations ($a_0 = 0$) and hence any Takens Bogdanov degeneracy. The Hopf condition can be rewritten as

$$(4u^2 - v^2)(4u^2 + \Delta^2)(u^2 + \Omega^2) - 2k^2u^2(4u^2 + 2\Omega^2 + \Delta^2/2) + u^2k^4 = 0.$$

The assumption that k is small restricts us to the following solution for k^2:

$$k^2 = 4u^2 + 2\Omega^2 + \Delta^2/2 - \sqrt{(2\Omega^2 - \Delta^2/2)^2 + (v/u)^2(4u^2 + \Delta^2)(u^2 + \Omega^2)},$$

with corresponding frequency

$$\omega^2 = \Omega^2 + \Delta^2/4 + u^2 - v^2/4 - k^2/2 + 2(v/u)\Omega\Delta.$$

Of special interest is the limiting case $v = 0$. In this limit the Hopf bifurcation occurs at

$$k^2 = 4u^2 + \Delta^2, \tag{17}$$

with frequency $\omega^2 = \Omega_1\Omega_2 - u^2$. The other limiting case is $\Delta = 0$ for which the Hopf bifurcation occurs at

$$k^2 = 4u^2 - 2\sqrt{\Omega^4 + v^2(u^2 + \Omega^2)} + 2\Omega^2.$$

We omit the computation of the nonlinear Hopf coefficient. The information about sub- or supercriticality of the bifurcating periodic orbit will be inferred from the amplitude-phase equations introduced in the next subsection.

3.2 Amplitude-phase equations

Since the two oscillators coupled in (4a) are identical except for their center frequencies, we can distinguish solutions with equal amplitudes and solutions with different amlitudes of the oscillators. To make this explicit, we introduce first polar coordinates $z_j = r_j e^{i\varphi_j}$ $(j = 1, 2)$ as in Section 2 and then switch to the coordinates

$$R = \frac{1}{2}(r_1^2 + r_2^2), \quad r = r_1^2 - r_2^2. \tag{18}$$

After averaging over the total phase Φ, (6a),(6b) specified to the case of (4a) transforms into the system

$$\begin{aligned}
\dot{R} &= 2uR + \frac{vr}{2} + \frac{1}{5}(4R^2 + r^2) - \frac{R}{10}(4R^2 + 3r^2) + \frac{k}{2}\sqrt{4R^2 - r^2}\cos\phi\,, \\
\dot{r} &= 2vR + 2ur + \frac{8}{5}Rr - \frac{r}{10}(12R^2 + r^2)\,, \\
\dot{\phi} &= \Delta + r(p + 2qR) - \frac{2kR}{\sqrt{4R^2 - r^2}}\sin\phi\,.
\end{aligned} \tag{19}$$

for R, r and the phase difference ϕ, with u, v as defined in (16) which are considered here as parameters.

In the remainder of this section we investigate the bifurcating solutions of (19) for $v = 0$. In this case the subspace $r = 0$, corresponding to equal amplitudes of the oscillators, is an invariant subspace for (19) which allows us to distinguish between "symmetric solutions" ($r = 0$) and "asymmetric solutions" ($r \neq 0$). The case $v \neq 0$ will be addressed in Section 4 in the context of the full system (4a)(4b). For simplicity, in order to have analytical access to the bifurcating solutions, we also set $p = q = 0$. Note that (19) with $v = 0$, $p = q = 0$ exhibits the reflection equivariance $(R, r, \phi) \to (R, -r, \phi)$.

When restricted to the invariant subspace $r = 0$, (19) reduces to

$$\dot{R} = 2uR + \frac{4}{5}R^2 - \frac{2}{5}R^3 + k\cos\phi \tag{20a}$$

$$\dot{\phi} = \Delta - k\sin\phi\,. \tag{20b}$$

Note that (20b) coincides with the phase equation (13) which was derived in the preceeding section in a more general setting. We mention that the system (20a),(20b) is also valid for $r = 0$ if p, q are nonzero.

3.3 Primary solutions and their bifurcations

We refer to the steady state solutions of (20a),(20b) as primary solutions (PS). For the original system (4a) PS correspond to periodic solutions with equal amplitudes but in general different phases of both oscillators. The equations $\dot{R} = 0$, $\dot{\phi} = 0$ are readily solved and yield the following parametric representation $K = K_p(R,u)$ and $\phi(R,u)$ of PS (we assume $k \geq 0$):

$$K_p = \delta + \frac{1}{4} f^2(R,u), \quad (\cos\phi, \sin\phi) = \frac{1}{2\sqrt{K_p}}(f(R,u), \sqrt{\delta}), \tag{21}$$

where

$$f(R,u) = R^2 - 2R - 5u, \tag{22}$$

and K, δ are the rescaled coupling and detuning parameters defined by

$$(K, \delta) = (25/16)(k^2, \Delta^2). \tag{23}$$

The bifurcation structure of (21) is easily discussed in terms of $f(R,u)$. There is a saddle node when $df/dR = 0$, i.e., at

$$R = 1, \ K = K_{SN_1} \equiv \delta + (1+5u)^2/4.$$

This saddle node, referred to as SN_1, is always present and involves the R-eigenvalue of the Jacobian. In addition there are saddle nodes when $f = 0$, i.e., at

$$R_\pm = 1 \pm \sqrt{1+5u}, \quad K = \delta,$$

which are referred to as SN_2. We see both R_+ and R_- when $0 > u > -1/5$ and only R_+ when $u > 0$. When $u < -1/5$ both $R_\pm$ have disappeared. The SN_2 correspond to saddle nodes on the ϕ-circle ($\phi = \pi/2$ or $3\pi/2$) and mark the boundary between the synchronized regime ($K > \delta$) and and the desynchronized regime ($K < \delta$).

The PS are created in a "primary bifurcation" (PB) from the basic state at

$$R = 0, \ K_{PB} = \delta + 25u^2/4.$$

This primary bifurcation is the basic Hopf bifurcation for (4a) and hence coincides with (17). In the amplitude-phase description it corresponds to a pitchfork. Sub- or supercriticality of the pitchfork can be deduced from the slope dK_p/dR at $R = 0$: for $u > 0$ the pitchfork is supercritical and for $u < 0$ it is subcritical. We note that at $u = -1/5$ there is a high degeneracy because both SN_2 and SN_1 coalesce. This high singularity can be resolved by introducing further mismatch parameters in the two oscillators which will, however, not pursued in this paper.

A further stability exchange involving the r-eigenvalue occurs at secondary bifurcations SB defined by $\partial\dot{r}/\partial r|_{r=0} = 0$ on PS, i.e., at $H(R,u)|_{PS} = 0$, where

$$H(R,u) = 5u + 4R - 3R^2. \tag{24}$$

The stability assignments along PS are easily found using the following information: at SN_2-points the ϕ-eigenvalue changes sign (once or twice), at SN_1 it is the R-eigenvalue and at SB the sign change involves the r-eigenvalue. Moreover, for large R all three eigenvalues are negative and close to PB we find the stability assignment from that of the trivial solution and the type (sub- or supercritical) of the pitchfork. The stability information will be summarized in bifurcation diagrams in Subsection 3.5.

The trivial solution (T) of (4a) has two complex conjugate pairs of eigenvalues, thus two signs suffice to fix the stability assignment: it is $--$ $(++)$ for $K < K_{PB}$ and $u < 0$ $(u > 0)$, and $+-$ for $K > K_{PB}$.

3.4 Secondary solutions and their bifurcations

Steady state solutions (R, r, ϕ) of (19) with $r \neq 0$ will be referred to as secondary solutions (SS). For the original system (4a) they correspond to periodic orbits with $r_1 \neq r_2$. Some algebra leads to the following parametric representation $K = K_s(R, u, \delta)$ and $\phi(R, u, \delta)$ along SS:

$$K_s = F(R,u)[(R-1)^2 + \delta/R^2], \quad (\cos\phi, \sin\phi) = \sqrt{F/K_s}(1-R, \sqrt{\delta}/R)\,, \tag{25}$$

where

$$F(R,u) = 4R^2 - 4R - 5u, \tag{26}$$

and r is given by $r^2 = 4H(R,u)$ on SS. The conditions $H \geq 0$, $F \geq 0$ define two parabolae in the (R,u)–plane such that SS is restricted to the region between these parabolae. The lower boundary $H = 0$ corresponds to the secondary bifurcation SB where SS branches off PS in a pitchfork bifurcation. Noting that $4R^2 - r^2 = 4F(R,u) = 4r_1^2 r_2^2$ on SS, the upper boundary $F = 0$ corresponds to the limit $r_1 \to 0$ or $r_2 \to 0$.

Besides SB the SS-branches show further steady state bifurcations of codimension up to three. First of all we find saddle nodes (SN) from $\partial K_s/\partial R = 0$, giving

$$R^3(R-1)(8R^2 - 10R + 2 - 5u) + \delta(2R + 5u) = 0\,. \tag{27}$$

The saddle nodes coalesce with SB giving rise to degenerate secondary bifurcations (dSB) if (27) and $H = 0$ hold simultaneously. These equations can be manipulated to yield a curve representation $\delta_{dSB}(R)$, $u_{dSB}(R)$, $K_{dSB}(R)$ $(2/3 < R \leq 1)$ defining the loci of these codimension two points in parameter space. If (25),(27) are augmented by the condition $\partial^2 K_s/\partial R^2 = 0$ we find

$$\delta^2 + R^2(4R-3)(6R^2 - 6R + 1)\delta - R^6(8R-5)(R-1)^2 = 0\,. \tag{28}$$

The equations (25),(27),(28) together yield cusp (or hysteresis) bifurcations, i.e., the coalescence of two saddle nodes. Again these equations can be manipulated to a curve representation $\delta_{cusp}(R)$, $u_{cusp}(R)$, $K_{cusp}(R)$ $(5/8 \leq R \leq 1)$ defing the loci of these codimension two points in parameter space. Finally, augmenting (25),(27),(28) by $\partial^3 K_s/\partial R^3 = 0$ we obtain a single equation for R,

$$80R^4 - 200R^3 + 176R^2 - 60R + 5 = 0, \tag{29}$$

with solution $R_{swal} = 0.7944$. The corresponding parameter values are found from (25),(27),(28): $\delta_{swal} = 0.1189$, $u_{swal} = -0.2534$, $K_{swal} = 0.5660$. This point marks a swallowtail point (codimension three) characterized by the coalescence of two cusp points. The numerical values of δ_{swal}, K_{swal} are relatively large, thus in the small coupling and detuning limit K and δ should be kept below these values (more precisely: in an asymptotic analysis fixed numerical values of the small parameter are not allowed). Still, however, the presence of the swallowtail point is a characteristic

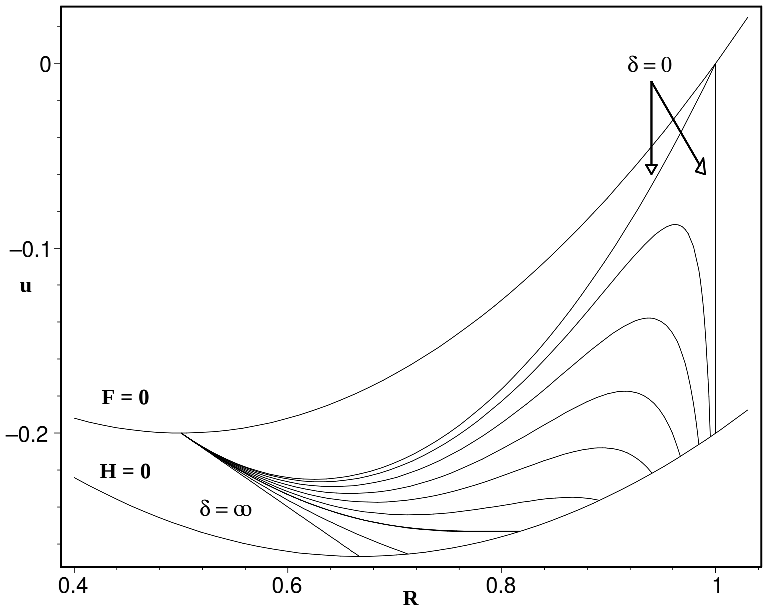

Figure 3: Projections of saddle node curves SN in the (u, R)-plane for $\delta = 0$ and δ=.005, .015, .03, .05, .08, .1182, .28. Also shown is the limit of these curves for $\delta \to \infty$. The SN–curves emanate from the minimum of the $(F = 0)$–parabola and terminate in dSB points on the $(H = 0)$–parabola. For $\delta = 0$ SN consists of a segment of a parabola and a vertical line segment at $R = 1$. When δ increases the dSB points move downwards and approach the $(H = 0)$–minimum for $\delta \to \infty$. The maxima and minima of the SN curves are projections of cusp points.

feature of the system (19) which we may just consider as *given*, i.e. not restricted to an asymptotic analysis. Coalescence of cusp and dSB-ponts, which also would be of codimension three, does not occur. In Figure 3 we show the (u, R)-plane and the projection of SN in that plane for some fixed, increasing values of δ.

Next we investigate Hopf bifurcations (H) of (19) on SS which correspond to torus bifurcations for (4a). The Jacobian of (19) with $v = p = q = 0$ along SS is calculated as

$$\frac{\partial(\dot{R}, \dot{\phi}, \dot{r})}{\partial(R, \phi, r)} = \frac{1}{5} \begin{pmatrix} a_{11} & \varepsilon a_{12} & a_{13} \\ \varepsilon a_{21} & a_{22} & \varepsilon \varrho a_{23} \\ \varrho a_{31} & 0 & a_{33} \end{pmatrix}, \tag{30}$$

with $\varepsilon = \sqrt{\delta}$ and

$$\begin{aligned} &a_{11} = 4R(1-R) - 4H\,, \quad a_{12} = -4F/R\,, \quad a_{13} = 1 - 2R\,, \\ &a_{21} = 4H/FR\,, \quad a_{22} = -4R(1-R)\,, \quad a_{23} = -1/F\,, \\ &a_{31} = 4(2-3R)\,, \quad a_{33} = -4H\,. \end{aligned}$$

The characteristic equation for an eigenvalue $\lambda \equiv 4\hat{\lambda}/5$ then takes the form

$$-\hat{\lambda}^3 - 2H\hat{\lambda}^2 - p_1\hat{\lambda} + Hp_0 = 0,$$

where

$$p_1 = H(5u - 10R^2 + 12R - 2) - R^2(1-R)^2 + \frac{\delta H}{R^2},$$
$$p_0 = R(1-R)(8R^2 - 10R + 2 - 5u) - \frac{\delta}{R^2}(5u + 2R).$$

The condition for a Hopf bifurcation, $\hat{\lambda} = i\omega$, is $2p_1 + p_0 = 0$ which can be rewritten as

$$\delta(5u + 6R - 6R^2) - R^2(2 - 5u - 12R + 10R^2)(10u + 7R - 5R^2) = 0. \quad (31)$$

The corresponding frequency is $\omega^2 = p_1$, thus we need $p_1 > 0$ (equivalently $p_0 < 0$). The third eigenvalue at a Hopf point is $-2H < 0$, hence the Hopf bifurcation creates a stable subbranch of SS. The bifurcating periodic orbit (torus for (4a)) can be stable or unstable, depending on the nonlinear Hopf coefficient which has not been calculated yet. The Hopf bifurcation degenerates to a Takens Bogdanov bifurcation TB if $p_1 = p_0 = 0$ ($p_0 = 0$ is the SN-condition). Together with (25), these equations yield a representation $\delta_{TB}(R)$, $K_{TB}(R)$, $u_{TB}(R)$ ($2/3 < R < 1$) of the codimension two TB-curve in parameter space. Finally, when the TB-conditions are augmented by the cusp condition (28) we find a single codimension three point in parameter space with coordinates $R_{TBc} = 0.7164$, $u_{TBc} = -0.2446$, $\delta_{TBc} = 0.0819$, $K_{TBc} = 0.0985$, where a cusp and a TB coalesce. There is another possibility for a codimension three version of TB which, however, requires a normal form computation. We have not attempted to check this condition because our simulations do not support the presence of such a degeneracy. The stabilities along SS are found in a similiar manner as for PS and will be summarized in the next subsection.

3.5 Bifurcation diagrams

We summarize our findings about stationary solutions of (19) for $v = 0$, $p = q = 0$ by presenting some typical, selected bifurcation diagrams. In Figure 4(a) a typical section through the bifurcation set in the (u, K)-plane is displayed with MAPLE showing the codimension one sets as curves and the codimension two sets as isolated points. Figure 4(b) shows an enlargement of a small region near the right cusp point of SN in which H emerges from the TB point. When δ increases, the qualitative forms of SN_1, SN_2, SB, PB remain basically the same, but several changes concerning SN and H occur. First, when δ passes through δ_{TBc}, TB moves to the lower of the two SN-branches joining at the right cusp. Then, for larger values of δ, the two cusps are both below SN_2 and coalesce and disappear in a "swallowtail event" when δ passes through δ_{swal}. We mention that SN_2 (which marks a saddle node of PS on the ϕ-circle) is actually doubly covered for u in the range $0 > u > -1/5$. In this range there is a single saddle node for the decoupled ϕ-variable, but associated with this saddle node are two different R-values. For $u > 0$ SN_2 is singly covered. The double covering of SN_2 is a degeneracy which is due to the specific choice of parameters. When further mismatches of the two oscillators are introduced the SN_2–line would unfold and split into several lines which likely will join in additional cusp points. We have not studied the resolution of this singularity.

In Figure 5 we show six typical bifurcation diagrams R versus K for fixed values of (δ, u). Note that (K, R)–diagrams correspond to vertical sections through (u, K)–diagrams such as that of Figure 4.

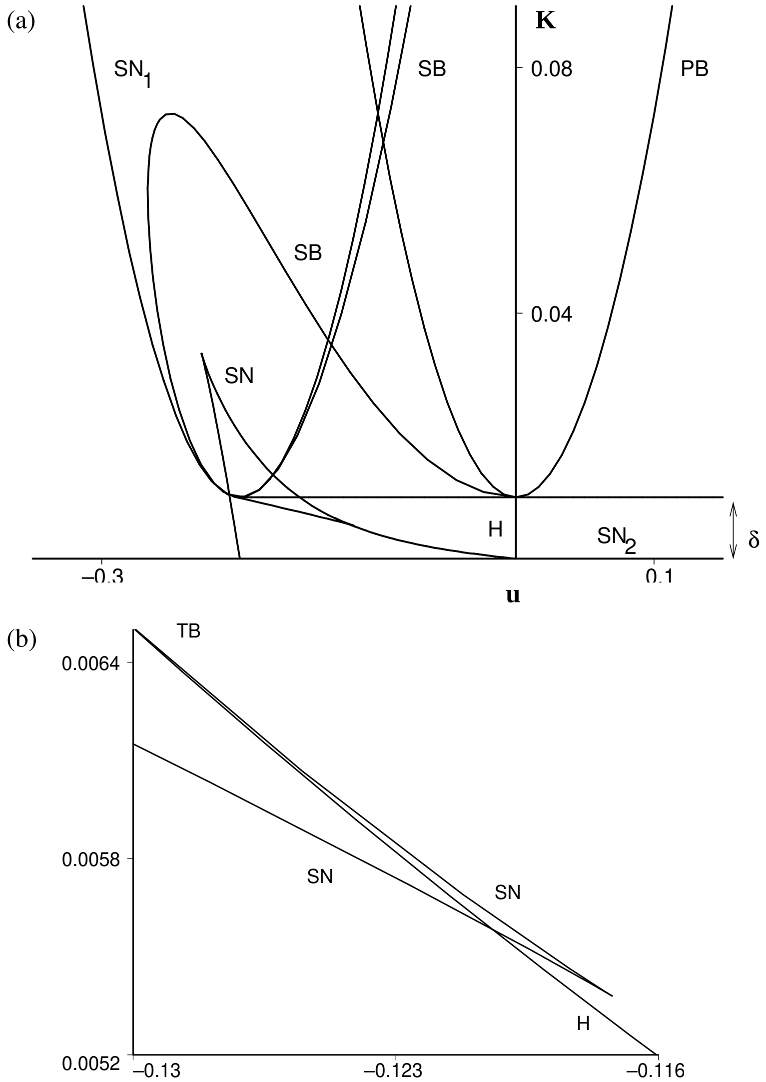

Figure 4: (a) Bifurcation set of stationary solutions of (19) in the (u, K)-plane for $\delta = 0.01$. Shown are PB: primary bifurcation of PS from the trivial state, SB: secondary bifurcation of SS from PS, $SN_{1,2}$: two different saddle nodes of PS, SN: saddle node of SS and H: Hopf bifurcation of SS. SN and H emanate tangentially from SB and SN at dSB and TB points, respectively. (b) Enlargement of a region near the right cusp of SN.

In all (R, K)–diagrams PS is always present whereas SS may or may not be present depending on (u, δ). In Figure 5(a) u is positive, hence only the upper SN_2–point appears. In this range there is only one SS-branch which is unstable. For $0 > u > -1/5$ PS exhibits two SN_2–points and the SN_1–point. There are now two disconnected SS–branches emanating from $K = 0$ (boundary $F = 0$) and terminating in SB–points on PS (Figure 5(b),(c)). In this regime there occurs a Hopf bifurcation (H) on the upper SS–branch (Figure 5(b)) which emerges at $K = 0$ ($u = 0$), moves

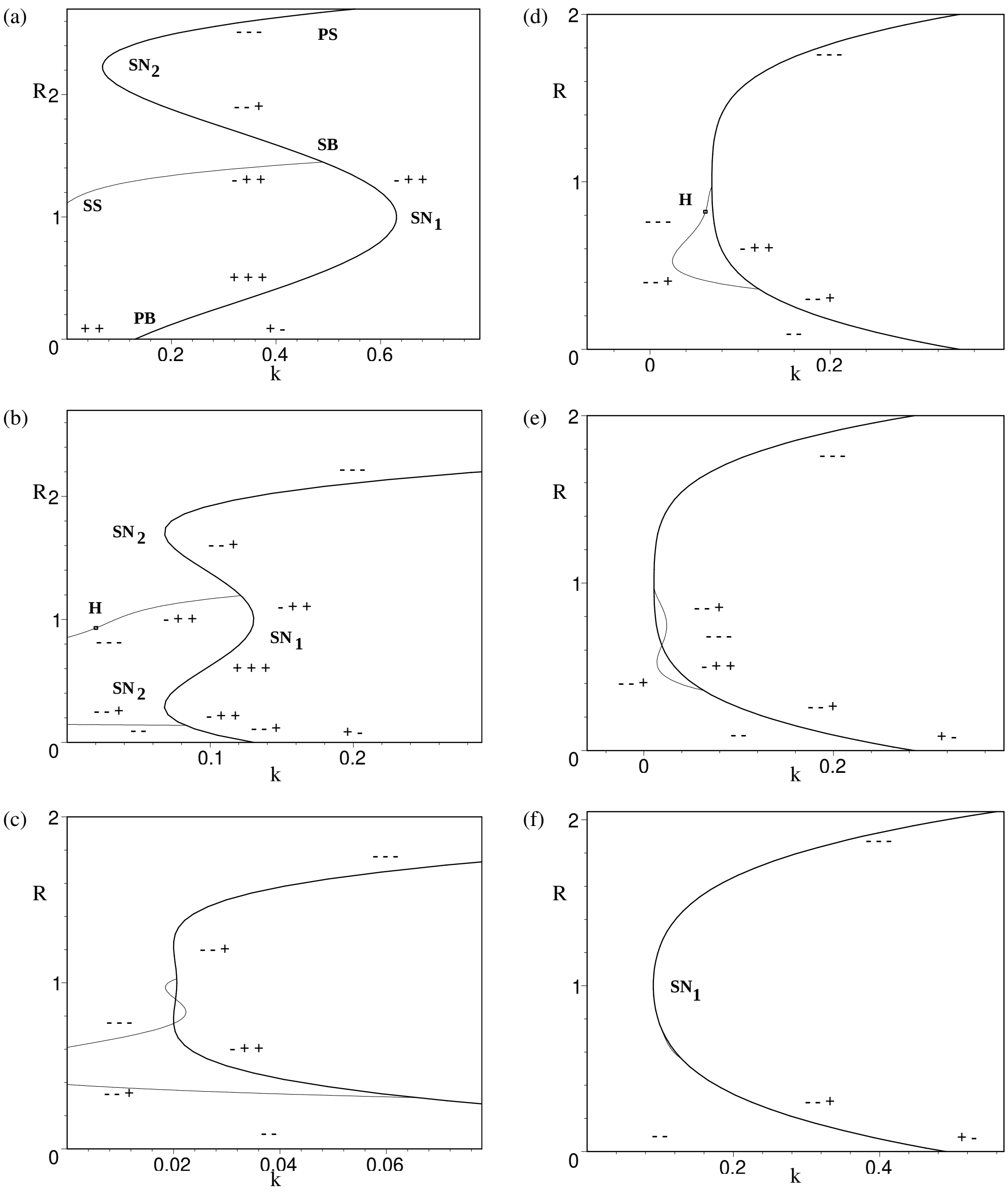

Figure 5: Typical bifurcation diagrams R (vertical) versus K (horizontal) showing primary (PS) and secondary (SS) steady state branches of (19) for $v = 0$, $p = q = 0$. The values of (u, δ) are (a): (.1,.068), (b): (-.1,.068), (c): (-.19,.02), (d): (-.21,.068), (e): (-.21,.01), (f): (-.26,.068). The signs attached to the various subbranches mark the stability assignments (signs of real parts of eigenvalues of the Jacobian). Also shown are the stability assignments (two signs) of the trivial solution $z_1 = z_2 = 0$ of (4a).

to the right when u increases and eventually is annihilated in a TB bifurcation, thereby creating a stable SS–subbranch. Before H reaches TB, clearly, SN–points have to be formed which can be due to dSB or a hysteresis (cusp). In Figure 5(c) the upper SS–branch is stable before the first SN is reached when K increases from zero. This diagram was also obtained with AUTO (Figure 2) for the original system (4a) which confirms that averaging over Φ is well justified. For $u < -1/5$ the two SN_2–points have disappeared leaving a single saddle node of type SN_1 on PS. In addition the former disconnected SS–branches join at an SN. Note that all of these transitions (coalescence of both SN_2's, SN_1 and the shrinking of SS to a single point) happen at $u = -1/5$, $K = 0$ which illustrates the highly singular nature of this point. For $u < -1/5$ there may (Figure 5(d)) or may not (Figure 5(e)) exist a Hopf point and up to two SN–points can occur. When u decreases further H and SN's disappear in succession leaving a monotonic SS–branch (stability assignment $--+$) that connects two SB's on PS below SN_1 and eventually disappears when u decreases further (Figure 5(f)).

In Figure 6 we show six typical bifurcation diagrams R versus u for fixed values of (K, δ). These diagrams correspond to horizontal sections through (u, K)-diagrams such as that of Figure 4. In the "desynchronized regime" ($K < \delta$, Figure 6(a),(b)) PS is not present, but we see SS which is partly stable in a bounded range due to the presence of H. For small K/δ there is only a single SN on SS (Figure 6(a)) while close to the "transition to synchrony" ($K = \delta$) three SN's occur (Figure 6(b)). In the "synchronized regime" ($K > \delta$, Figure 6(c)-(f)), the diagrams are dominated by two disconnected PS-branches emanating in succession from the trivial solution in PB's. Both of them have a single saddle node of type SN_1 above which the left PS-branch is stabilized. In addition there is always an unbounded, unstable SS-branch which is created in an SB-point on the right PS-branch. For K/δ not too large we also see another SS-branch joining two SB-points on the PS-branch (Figure 6(c)-(e)), similarly as in the (K, R)-diagrams of Figure 5. Here again up to two SN-points as well as an H-point can be present (Figure 6(c),(d)) giving rise to a stable portion of the bounded SS-branch. When K increases, H and the SN's disappear due to TB and dSB or a cusp, respectively, leaving an unstable bounded SS-branch joining two SB's (Figure 6(e)). Further increase of K causes the two SB's to merge such that the bounded SS-branch disappears (Figure 6(f)). Note that in the (u, R)-bifurcation diagrams we do not see a saddle node of type SN_2 on PS. This saddle node is only seen for $K = \delta$ when the two PS-branches merge and disappear. At this point the full degenerate PS-branch is of type SN_2 which is a special feature of our system and will be resolved when further mismatch parameters are introduced.

3.6 Rotating solutions

By rotating solutions we understand periodic solutions of (19) with full rotation of $\phi \bmod 2\pi$ around its circle. For the original system (4a) rotating solutions correspond to distinguished quasiperiodic solutions along which, loosely speaking, the phase of one oscillator repeatadly "overtakes" the phase of the other oscillator. We distinguish again between primary rotating solutions (PRS) located in the invariant plane $r = 0$ and secondary rotating solutions (SRS) located off that plane.

In the small coupling limit a rotation of ϕ induces a small periodic perturbation of the (R, r)-system with $k = 0$. Since this system is dominated by the fixed points (in the original coordinates r_1, r_2 it is decoupled), rotating solutions for small k are revealed as oscillations about fixed points of the (R, r)-system for $k = 0$, at least as long these fixed points are hyperbolic. Thus we can study rotating solutions by expanding (19) about the different types of fixed points of the (R, r)-system

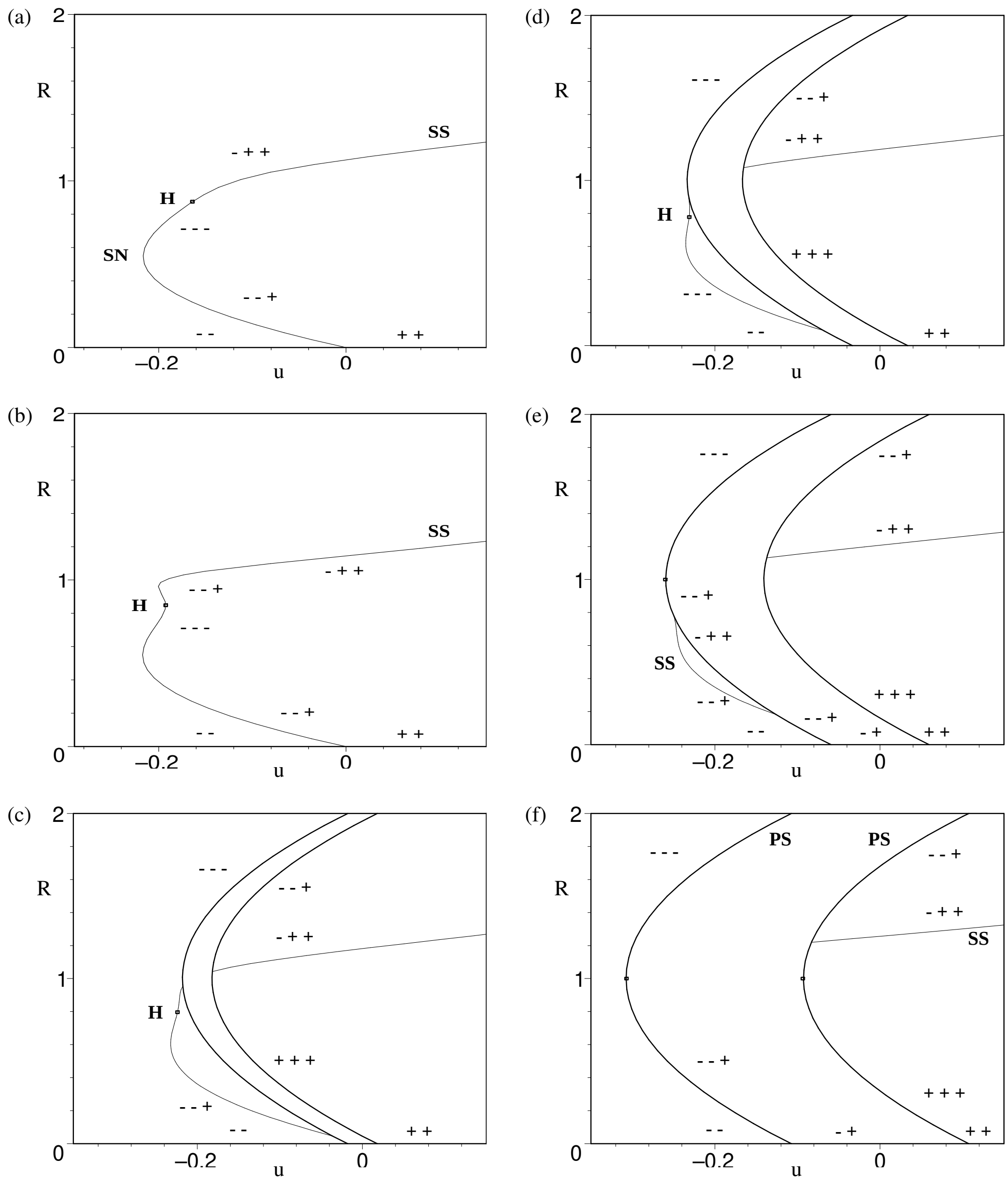

Figure 6: Typical bifurcation diagrams R (vertical) versus u (horizontal). The values of (K, δ) are (a): (.04,.068), (b): (.029,.03), (c): (.07,.068), (d): (.075,.068), (e): (.09,.068), (f): (.14,.068). Meaning of branches, bifurcation points and stability assignments as in Figure 5.

for $k = 0$. These are the trivial fixed point $R = r = 0$, and

$$\begin{aligned} PS_0 : &\quad r = 0,\ f(R,u) = R^2 - 2R - 5u = 0, \\ SS_0 : &\quad r^2 = 4R^2,\ F(R,u) = 4R^2 - 4R - 5u = 0, \\ SS_1 : &\quad R = 1,\ r^2 = 4(5u+1) \quad (-1/5 \le u \le 0). \end{aligned}$$

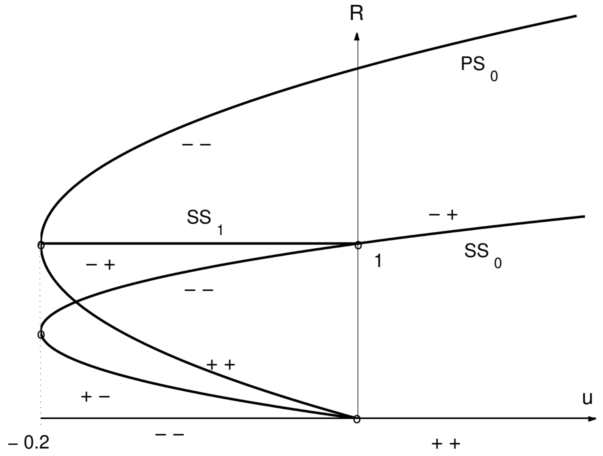

Figure 7: (R, u)–Bifurcation diagram for $k = 0$ showing the trivial solution and PS_0, SS_0, SS_1 and their stability assignments.

On PS_0 both oscillators have the same amplitude ($r_1 = r_2$), on SS_0 one oscillator is at rest and the other oscillates ($r_1 = 0$, $r_2 \neq 0$ or vice versa) and on SS_1 one oscillator is in its stable oscillation and the other is in its unstable oscillation. In Figure 7 the projection of these solution branches in the (R, u)-plane are shown. Note that in three dimensions PS_0 is located in the invariant plane $r = 0$, SS_0 consists of two symmetrically related branches located in the "boundary planes" $r = \pm 2R$ and SS_1 connects the saddle node of PS_0 to the two branches of SS_0 at $u = 0$.

The analytical study of rotating solutions is a delicate matter and a complete, rigorous analysis would be beyond the scope of this paper. We confine ourselfes to some special cases which allow an easy analytical approach. First we study generic points of some of the branches of Figure 7 and then we investigate neighborhoods of the two bifurcation points of SS_1.

3.6.1 Generic PS_0-points.

We choose R_0, the R-coordinate of a PS_0-point, as parameter, i.e., $5u = R_0^2 - 2R_0$, and set $R = R_0(1 + \varrho)$. Expanding (19) about $(\varrho, r) = (0, 0)$ yields at leading order

$$\dot{\varrho} = \alpha\varrho + k\cos\phi, \quad \dot{r} = \alpha r, \quad \dot{\phi} = \Delta - k\sin\phi, \tag{32}$$

where $\alpha = 4R_0(1 - R_0)/5$ must be nonzero. Thus consistent with the phase description of Section 2 we find primary rotating solutions PRS ($r = 0$) for $k < \Delta$ which are stable for $R_0 > 1$ (both oscillators in their stable oscillation) and unstable in both the ϱ- and the r-direction for $R_0 < 1$ (both oscillators in their unstable oscillation).

Let $\phi_{rot}(t)$, $\varrho_{rot}(t)$ ($r = 0$) be the rotating solution to (32). Since the average of $\cos\phi_{rot}(t)$ is zero, the average of $\varrho_{rot}(t)$ is zero as well. If k/Δ is small, a rough approximation for $\varrho_{rot}(t)$ is provided by

$$\varrho_{rot}(t) \approx \frac{k}{\alpha^2 + k^2}[\Delta\sin(\Delta t) - \alpha\cos(\Delta t)],$$

which can be improved, for example, by Linstedt's method. When Δ/k is $O(1)$ this formula is no longer valid, but the average of $\varrho_{rot}(t)$ still vanishes (at least up to $O(k)$). In the limit $k/\Delta \to 1$ PRS then encounters an infinite period bifurcation where it joins the PS-steady state branch at an SN_2-point.

Due to the zero average of $\varrho_{rot}(t)$, the averages of the rotating solutions in the $(r = 0)$-plane can, up to $O(k)$, be identified with the PS_0-branches. The (R, K) bifurcation diagrams (a),(b),(c) of Figure 5 (fixed $u > -1/5$) may then be augmented by horizontal PRS-branches $R = R_0$ joining $K = 0$ and SN_2, with stability assignments $--$ for $R_0 > 1$ and $+-$ for $R_0 < 1$. Similarly, the (R, u)-diagrams (a),(b) of Figure 6 can be augmented by the PS_0-branch of Figure 7 which here plays the role of a PRS-branch. The stability assignments of this branch are the same as the PS_0-assignments in Figure 7 as long as we stay away from the saddle node at $u = -1/5$. Below we will study the "unfolded" $(k \neq 0)$ version of this saddle node point.

3.6.2 Generic SS_0-points

These do not unfold to rotating solutions for small $k \neq 0$ which can be seen from the ϕ-equation of (19): SS_0 is located on the boundary $r^2 = 4R^2$, thus for $k \neq 0$ we can expect the term multiplying $\sin\phi$ in (19) to be large and hence to induce a steady state rather than a rotating solution. This rough argument can be made more rigorous by a perturbation analysis. However, since one oscillator is at rest on SS_0, its phase and hence ϕ is not defined. The perturbation analysis must, therefore, be carried out for the original system (4a). The starting point is then (4a) rewritten in polar coordinates for z_1, say, and in the original (complex) coordinates for z_2. Expanding r_1 about a nonzero amplitude r_0, i.e. $u = r_0^2(r_0^2 - 2)/5$, and z_2 about $z_2 = 0$ leads at leading order to

$$\dot{\varrho} = \alpha\varrho + \frac{ky}{r_0}\sin\varphi, \;\; \dot{\varphi} = \Omega_1 + \frac{ky}{r_0}\cos\varphi, \;\; \dot{z} = (u + i\Omega_2)z + ikr_0\sin\varphi, \tag{33}$$

where $r_1 = r_0(1 + \varrho)$, $\varphi = \varphi_1$, $z = z_2$, $y = \mathrm{Im}(z)$ and $\alpha = 4r_0^2(1 - r_0^2)/5$. It is then an easy matter to construct (up to $O(k)$) the return map of this system with respect to φ and to show that this map has a unique fixed point $(\varrho, z) = O(k)$ when $u \neq 0$ and $\alpha \neq 0$. Clearly this fixed point corresponds to a phase locked oscillation of (4a) and hence to a steady state with $r \neq 0$ for (19).

3.6.3 Generic SS_1-points

Introducing incremental variables $r = 2\sqrt{5u + 1}(1 + s)$ and $R = 1 + \varrho$ about a generic SS_1-point $(0 > u > -1/5)$, we obtain at leading order

$$\begin{aligned} \dot{\varrho} &= -\frac{4}{5}(5u + 1)(\varrho + s) + k\sqrt{-5u}\cos\phi, \\ \dot{s} &= -\frac{4}{5}[(5u + 1)s + \varrho], \;\; \dot{\phi} = \Delta - \frac{k}{\sqrt{-5u}}\sin\phi. \end{aligned}$$

These equations confirm that the underlying SS_1-point is a saddle and, moreover, that phase locking occurs if

$$\frac{k^2}{\Delta^2} = \frac{K}{\delta} = -5u. \tag{34}$$

From this we conclude that the SS_1-branch unfolds partly to SS and partly to SRS. Checking with the SS-representation (25) shows that (34) together with $\phi = \pi/2$ marks indeed a point on the SS-branch, but is consistent with the SN-condition (27) only if $\delta = 0$. The condition (34) can be corrected perturbatively to higher order in K and yields a bifurcation point on SS from which a rotating solution SRS of saddle type branches off. The nature of this branch point is not fully clear yet. It may be a homoclinic point or an infinite period bifurcation (coalescence of SRS with a saddle node of SS as for PSS and PS). Since in any case the period goes to infinity we refer to it as IP.

3.6.4 Saddle node on PS_0

At $u = -1/5$ there is a coincidence of a secondary bifurcation of SS_1 from PS_0 and a saddle node on PS_0. Our goal is to find the separation of these bifurcations for $k \neq 0$ and to determine the type (super- or subcritical) of the secondary bifurcation. A particularly easy approach to resolving this singularity is accessible when $k \ll \Delta$. Thus we assume that $0 < -(5u+1) \ll k \ll \Delta$ and treat Δ as $O(1)$-quantity. Introducing a small parameter ε, the appropriate perturbation variables are

$$5u + 1 = -\varepsilon^2, \;\; k = \frac{2}{5} q\varepsilon, \;\; \Delta = \frac{2}{5} d, \;\; R = 1 + \varepsilon\varrho, \;\; r = 2\varepsilon s,$$

with (q, d) considered as $O(1)$-parameters (the numerical factors have been introduced for convenience). The system (19) is expanded up to $O(\varepsilon^3)$,

$$\begin{aligned}
\frac{5\dot{\varrho}}{2} &= q\cos\phi + \varepsilon(1 - \varrho^2 - s^2 + q\varrho\cos\phi) + \varepsilon^2(\varrho - \frac{3\varrho s^2}{4} - \varrho^3 - \frac{qs^2}{2}\cos\phi) + \frac{\varepsilon^3 q\varrho^3}{2}\cos\phi + O(\varepsilon^4), \\
\frac{5\dot{s}}{2} &= -2\varepsilon s\varrho - \varepsilon^2 s(1 + s^2 + 3\varrho^2), \\
\frac{5\dot{\phi}}{2} &= d - \varepsilon q\sin\phi - \frac{\varepsilon^3 qs^2}{2}\sin\phi + O(\varepsilon^4),
\end{aligned}$$

which we rewrite as

$$\begin{aligned}
\frac{d\varrho}{d\phi} &= \frac{q}{d}\cos\phi + \frac{\varepsilon}{d}(\frac{q^2}{2d}\sin 2\phi + 1 - \varrho^2 - s^2 + q\varrho\cos\phi) + \varepsilon^2 p_2 + \varepsilon^3 p_3 + O(\varepsilon^4), \\
\frac{ds}{d\phi} &= -\frac{2\varepsilon s\varrho}{d} - \frac{\varepsilon^2 s}{d}(1 + 3\varrho^2 + s^2 + \frac{2q\varrho}{d}\sin\phi) + O(\varepsilon^3).
\end{aligned}$$

The higher order terms p_2, p_3 are lengthy expressions depending on $(\varrho, s^2, \sin\phi, \cos\phi)$ which we do not write down explicitely. One possibility to study this system is to apply the averaging method. However, it turns out that higher order expansions are necessary and the higher order terms are more easy to handle if a map description is used which is the approach we follow here.

The (ϱ, s)-system is easily solved perturbatively for given initial conditions,

$$\varrho(\phi, \varrho_0, s_0) = \varrho_0 + \frac{q}{d}\sin\phi + \dots, \;\; s(\phi, \varrho_0, s_0) = s_0 + \dots,$$

from which we can construct the return map

$$(\varrho_0, s_0) \to (\varrho(2\pi), s(2\pi)) = (\varrho_0, s_0) + \frac{2\pi\varepsilon}{d}(g(\varrho_0, s_0^2, \varepsilon), s_0 h(\varrho_0, s_0^2, \varepsilon)).$$

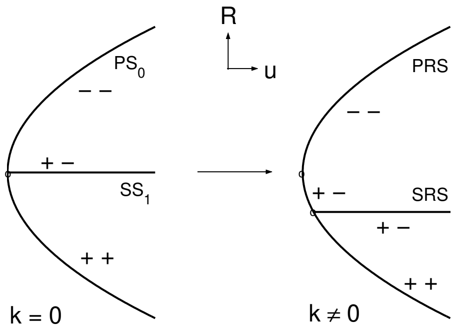

Figure 8: Unfolding of the saddle node on PS_0 for $0 < k \ll \Delta$.

The leading term of g is given by

$$g = 1 - \frac{q^2}{2d^2} - \varrho_0^2 - s_0^2 + O(\varepsilon),$$

which tells that at leading order a saddle node of PRS, referred to as SN_r, occurs at $\varrho_0 = 0$ when $q^2/2d^2 = 1$. We therefore introduce a further small parameter η by setting $q = \sqrt{2}d(1-\eta)$. Computation of the $O(\varepsilon)$- and $O(\varepsilon^2)$-terms of g shows that these terms vanish when $(\varrho_0, s_0, \eta) = (0,0,0)$. This greatly simplifies the analysis and allows us to infer all relevant local information about the bifurcations from the following expansions of g, h:

$$\begin{aligned} g &= 2\eta - \varrho_0^2 - s_0^2 - 6\varepsilon\varrho_0 + O(\eta^2, \varepsilon s_0^2, \varepsilon\varrho_0^2, \varepsilon\eta, \varepsilon^2\varrho_0, \varepsilon^3) \\ h &= -2\varrho_0 - 8\varepsilon + O(\varepsilon\eta, \varepsilon\varrho_0, \varepsilon s_0^2, \varepsilon^2). \end{aligned}$$

First we determine SN_r by solving $(g, \partial g/\partial\varrho_0) = (0,0)$. The corrected SN_r-coordinates are easily found as

$$SN_r: \quad \varrho_0 = -3\varepsilon + O(\varepsilon^2), \ \ \eta = -9\varepsilon^2/2 + O(\varepsilon^3),$$

and the s-eigenvalue of the (ϱ_0, s_0)-map at SN_r is given by $1 - 2\varepsilon + O(\varepsilon^2) < 1$.

Next we determine the secondary bifurcation where SRS branches off PRS which will be referred to as SB_r. The coordinates of SB_r are found from $(g,h) = (0,0)$ which has the solution

$$SB_r: \quad \varrho_0 = -4\varepsilon + O(\varepsilon^2), \ \ \eta = -4\varepsilon^2 + O(\varepsilon^3).$$

To determine the type of the SB_r-pitchfork we set $\varrho_0 = -4\varepsilon(1+\varrho_1)$, $\eta = -4\varepsilon^2(1-\eta_1)$ and $s_0 = \varepsilon s_1$. Solving then $g = 0$ yields $\varrho_1 = \eta_1 - s_1^2/8 + h.o.t.$ and substituting this into $s_0 h/\varepsilon^2 = 0$ leads to the pitchfork normal form $s_1(8\eta_1 - s_1^2) + h.o.t. = 0$, i.e., the pitchfork is supercritical. Thus the coincident saddle node and secondary bifurcation point on PS_0 unfolds into SN_r and SB_r as shown in Figure 8.

3.6.5 Bifurcation of SS_1 from SS_0

Our last local investigation concerns the point $u = 0$, $r^2 = 4$, $R = 1$ where SS_1 branches off SS_0. Choosing $r = 2$, for $k = 0$ the first oscillator is in its stable oscillation while the second oscillator is at rest. Thus φ_2 is not defined and we have to use equation (33) of Subsection 3.6.2, but with the cubic term $2z^2\bar{z}/5$ included for the second oscillator. We can approximately set $\varphi = \Omega_1 t$ and, since $\alpha = -48/5$ has a fixed, negative value, $\varrho = -(k/\alpha r_0)\sin(\Omega_1 t)$. What remains is a periodically forced version of a subcritical Hopf bifurcation,

$$\dot{z} = (u + i\Omega_2)z + \frac{2}{5}z^2\bar{z} + ikr_0\sin(\Omega_1 t) \tag{35}$$

for the second oscillator. The supercritical (stable) version of this system has been studied by Kath (1981) using a multiple scale expansion. The appropriate slow and fast times are (in our notation)

$$t^* = (\Omega_2 + \beta k^{2/3})t, \;\; \tau = k^{2/3}t,$$

and the frequency mismatch is described by $\Omega_1 - \Omega_2 = \beta k^{2/3}$, u is rescaled as $u = -\sigma k^{2/3}$ and $z(t)$ is expanded as

$$z(t) = k^{1/3}s(\tau)\cos(t^* + \theta(\tau)) + O(k^{2/3}).$$

In our unstable situation the resulting slow system for $s(\tau)$, $\theta(\tau)$ of Kath reads

$$\frac{ds}{d\tau} = s^3 - \sigma s - \sin\theta, \;\; s\frac{d\theta}{d\tau} = \beta s - \cos\theta,$$

with (β, σ) considered as $O(1)$–bifurcation parameters. Clearly, steady states of the (s, θ)-system correspond to SS and periodic solutions with θ winding about its circle correspond to SRS. Kath finds two saddle nodes of steady states and the creation of SRS in an infinite period bifurcation at one of the saddle nodes. In addition he shows the presence of oscillating periodic solutions (θ not rotating) created in a Hopf bifurcation and terminating in a homoclinic bifurcation which are both organized by a Takens Bogdanov bifurcation. These results match perfectly to our global bifurcation analysis of SS and may be used to partly augment our SS-bifurcation diagrams by SRS and oscillating solution branches. We refer to the paper of Kath (1981) for details. Note that in our subcritical situation all periodic solutions are unstable.

In summary we find PRS which are stable over full parameter ranges whereas SRS as well as the oscillating periodic solutions generated at H-points seem to be unstable, at least in the studied parameter regimes. This is in agreement with our observations made in a number of simulations for both the original four-dimensional system (4a) and the reduced three-dimensional system (19).

4 Implications for coupled elliptic bursters

4.1 Slow dynamics and synchronization

When we examine the fast time scale of a singularly perturbed differential equation, the system appears as a perturbation of a family of vector fields

$$\dot{x} = f(x, u), \qquad u = \text{const.}, \tag{36}$$

parameterized by the slow variable u. The perturbation parameter induces a slow variation of the parameters, producing a slowly varying system. If the quasistatic approximation (36) has a family of attractors depending smoothly on the parameter u, the solutions of the original system should be close, at any time, to the attractor of (36). Bifurcations in the family of vector fields induce transitions of trajectories from the neighborhood of one family of attractors to another on the fast time scale. Trajectories of the singular perturbed vector field can be decomposed into segments during which the trajectories remain in invariant sets of the fast subsystem, called *slow manifolds*, and segments in which the trajectories makes fast jumps between the invariant sets.

A single burster ($\mu \neq 0$) has two 1-dimensional slow manifolds, the steady state $r = 0$ and the primary branch generated in the Hopf bifurcation. Recall that fixed points of (3) are determined by intersections of the Hopf branch with $r^2 = a$ and the fixed point is stable for $a > 1$. The bifurcation analysis of Section 3 can be extended to coupled bursters by supplementing (19) by the equations determining the evolution of the slow variables u and v. In terms of (R, ϕ, r) the equations (4b) become

$$\dot{u} = \mu(a - R), \quad \dot{v} = -\mu r, \tag{37}$$

and the invariant plane $r = 0$ of the fast subsystem is now extended to the three–dimensional invariant subspace (R, ϕ, u). In the 5-dimensional system (R, ϕ, r, u, v) the slow manifolds are 2-dimensional and since $\dot{v} = -\mu r$, equilibrium solutions can only exist in the invariant subspace (R, ϕ, u) and are determined by intersections of the plane $R = a$ with the primary solution branch PS for $K > \delta$. Since $r \neq 0$ on the secondary branches SS, these do not contain any fixed points. For $K < \delta$ there are no fixed points since there is no primary branch.

The stability of the dynamics on the slow manifold in (R, ϕ, u) can be inferred from the Jacobian evaluated along PS. Of particular interest is now the 2×2 matrix M,

$$M = \frac{\partial(\dot{r}, \dot{v})}{\partial(r, v)} = \begin{pmatrix} \lambda & 2R \\ -\mu & 0 \end{pmatrix}, \tag{38}$$

where $\lambda = \partial\dot{r}/\partial r$, which determines the stability against perturbations that are transversal to (R, ϕ, u). Recall that, when considering the reduced fast subsystem for $v = 0$, $\lambda = 0$ yields secondary bifurcations. In the extended system, when u, v are treated as dynamical variables, $\lambda = 0$ induces now an imaginary eigenvalue because $\det M = 2\mu R > 0$. Thus secondary bifurcation points (SB) of the fast subsystem mark the occurence of superimposed slow oscillations in the full fast–slow system. To get an idea how these oscillations are revealed consider a neighborhood of an SB–point with u–coordinate u_{SB} and let $\Delta u = u - u_{SB}$. For $v = 0$ the bifurcation diagram in $(r, \Delta u)$ is a pitchfork due to the symmetry $r \to -r$. Assume that this pitchork is supercritical as indicated by the flow directions in Figure 9(a).

When variations of v are taken into account the reflection symmetry is broken and locally the projection on $(r, \Delta u, v)$–space of the two–parameter family of fixed points of the fast subsystem forms the surface of an "overhanging cliff" (cusp–surface) familiar from catastrophe theory (Poston and Stewart, 1978). Before the bifurcation (fixed $\Delta u < 0$) the corresponding (r, v)–section looks as shown in Figure 9(b), where $r \to 0$, $v \to 0$ due to the slow motion. After the bifurcation (fixed $\Delta u > 0$) we see a hysteresis and hence a relaxation oscillation consisting of slow drifts and fast transitions as illustrated in Figure 9(c). Thus in general we can expect u–drifts along the SS–branches with superimposed oscillations in (v, r) whose averages are approximately at $r = 0$, $v = 0$ due to the symmetry $(r, v) \to (-r, -v)$. Consequently the projections of the SS–branches onto the invariant subspace (R, ϕ, u) play the role of averages of the superimposed slow oscillations.

It is worth to mention that the (v, r)–oscillations are a consequence of the fact that the slow subsystems of both oscillators are also identical ($a_1 = a_2 = a$). A small mismatch of a_1, a_2 will

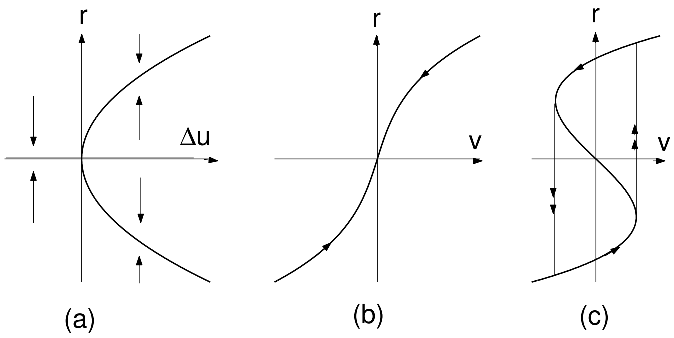

Figure 9: (a) Supercritical $(\Delta u, r)$–bifurcation diagram near an SB–point for $v = 0$. When $v \neq 0$ this diagram unfolds to a surface in $(\Delta u, v, r)$–space with (v, r)–sections as shown in (b) and (c) for fixed $\Delta u < 0$ and $\Delta u > 0$, respectively, giving rise to slow motions and fast transitions for $\mu > 0$.

introduce a nonzero real part of the imaginary eigenvalue of the (v, r)–system at SB and so will lead to a superslow (timescale $\mu|a_1 - a_2|$) growth or decay of the slow oscillations, at least in the vicinity of SB–points. In this paper we do, however, not study the effect of such a mismatch further.

As shown in Figure 6(c)-(f), when $K > \delta$ we find a stable PS above SN_1 ($R = 1$) on the left of the two PS–branches. Thus when $a < 1$ we see a similiar behaviour as for a single burster, namely a stable slow limit cycle consisting of the stable PS–branch and the trivial solution, restricted to $u_{SN_1} < u < 0$, with fast transitions between these slow manifolds. Along this limit cycle we find full burst synchronization combined with slow interspike desynchronization because ϕ variies with u. In addition a stable segment of SS (Figure 6(c),(d)) may be present with its slow relaxation oscillations as described before. If $a < R_{SN}$ (the R–coordinate of the saddle node SN on SS) an initial point on the stable SS–segment will drift along SS across SN and the dynamics will be captured by the slow (R, ϕ, u)–limit cycle. Only if $R_{SN} < a < 1$ we may find an attracting state involving the stable portion of SS. Then (R, u) will be frozen into some neighborhood of $R = a$, $u = u_{SS}(a)$ where $u_{SS}(R)$ is the parametrization u versus R on SS. The dynamics of such a state is dominated by the (r, v)–oscillations and hence leads to both burst and interspike desynchronization without a quiescent phase. In fact, such a state is characterized by alternating strong activities of the two bursters. However, finding such a state requires considerable fine tuning and we did not succeed yet in finding this state for $k > \Delta$, but observed alternating activities for $k < \Delta$ (see Figure 11 below).

Things would change drastically if SB would appear on the stable part of PS above SN_1. Then the former (R, ϕ, u)–limit cycle would also contain a segment of SS and we would see initially burst synchronization, but before the quiescent phase sets in a burst desynchronization would occur due to the drift along SS. The choice of parameters made in this paper excludes this possibility, however, with $p, q \neq 0$ and additional mismatches of the two oscillators imperfect versions of this scenario (a clear distinction between primary and secondary solutions is then no longer possible) are likely to occur. This will be the subject of another investigation.

In the desynchronized regime $k < \Delta$ the role of PS is taken by the primary rotating solution PRS. Thus we will find the same kind of cycle as before, but now combined with a rotation of ϕ, hence we expect burst synchronization and fast interspike desynchronization. Moreover, in this case we have a three–frequency motion for the original system (4a),(4b) and hence the three–torus should break up into two–tori and chaotic attractors leading to a complex structure of the interspike dynamics. In addition we find stable portions of SS giving rise to burst desynchronization for appropriate initial conditions and suitable values of a as in the synchronized regime. Concerning the secondary rotating solutions SRS, these branches seem to be unstable throughout and so are not expected to become slow pieces of attracting states. For more general choices of parameters the role of SRS may change, but this requires further investigation.

In summary, the fast–slow dynamics will be dominated by slow manifolds in (R, ϕ, u)–space consisting of the trivial state and a stable segment of PS or PRS. The cycles associated with these slow manifolds are both characterized by burst synchronization as in the case of fully identical bursters studied by Izhikevich (2000a; 2000b). Only for special initial conditions and parameters we may find burst desynchronization. Further mismatch parameters besides Δ have to be introduced in order that burst desynchronization becomes the dominant feature of coupled elliptic burster dynamics in certain parameter regimes.

4.2 Simulations

For the simulations and the numerical investigations using AUTO the fast subsystem (4a) was transformed into cartesian coordinates. All performed simulations of (4a), (4b) confirm the main conclusion of the preceeding subsection that, in accordance with the results of Izhikevich (2000b; 2000a) for identical bursters, burst synchronization in coupled elliptic bursters is difficult to avoid. It can be observed for arbitrarily small values of coupling strength. A frequency mismatch $\Delta = \Omega_1 - \Omega_2$ does not change this behavior significantly. By increasing coupling strength both bursters adjust their spiking frequencies until they adapt a common frequency at k_c, where we found complete burst and spike synchronization. For small and intermediate values of k compared to the detuning Δ we can observe different bursting patterns. Typically, here we found burst synchronization with quasiperiodic spiking. The observed behavior can be easily explained by the bifurcation structure of the fast subsystem. Simulations of the corresponding dynamics in the parameter regimes as in Figure 6(a), (b) and (d) are shown in the figures 10, 11 and 12, respectively. The figures show in (a) the bursting patterns of the imaginary parts $y_i(t)$, in (b) the evolution of the amplitudes $r_i(t)$ over time, in (c) a projection on (R, u), in (d) a projection on (r_1, r_2), and in (e) the evolution of the full system in the phase space spanned by the variables (x_1, y_1, u). As shown in Figure 6(a) and (b) in the "desynchronized regime" for $k < \Delta$ PS is not present and we see SS which is partly stable in a bounded range due to the presence of H. In Figure 11 the stable SS and H give rise to burst desynchronization without a quiescent phase as described above. In Figure 10 the additional saddle nodes close to H just modify the firing patterns during the active phase. Figure 12 shows the perfect burst and spike synchronization for $K > \delta$.

Of particular interest is the behavior when the secondary branches are partly stable or unstable due to the secondary Hopf bifurcation H as can be observed in the Figures 2 or 5 at values $k < \Delta$. For example, in parameter regimes for k were SS is unstable we can observe that both bursters transmit on their intrinsic frequency, without a significant influence from the other burster,

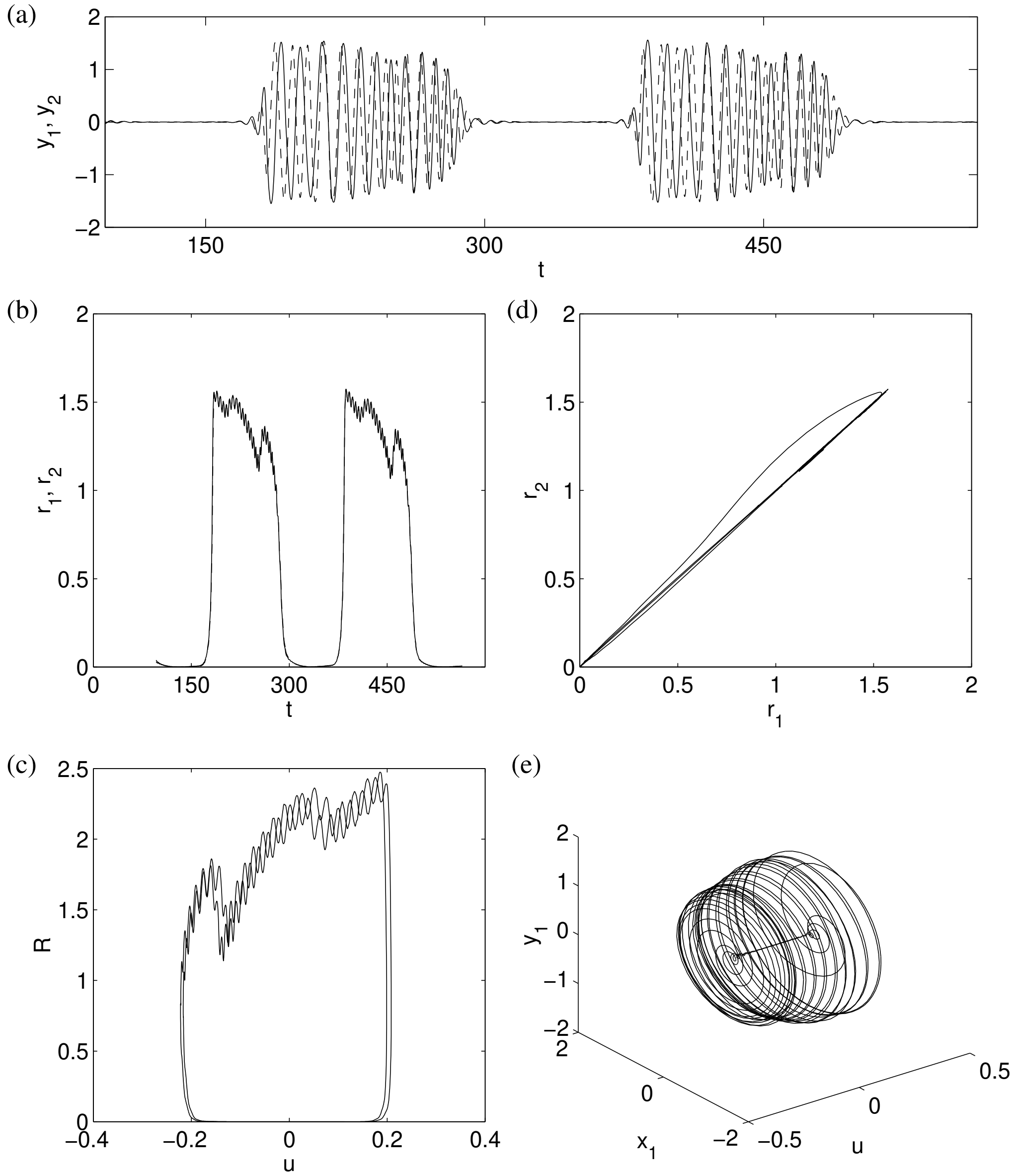

Figure 10: Two coupled elliptic bursters. Parameters as in Figure 6(b): $K = 0.029$, $\delta = 0.136$ ($\Omega_1 = 1$, $\Omega_2 = 0.7914$, $a = 0.79$, $b = 0.2$, $\mu = 0.005$, and $k = 0.16$). (a) Bursting patterns of the variables $y_i(t)$, (b) amplitudes r_i over time, (c) projection on (R, u), (d) projection on (r_1, r_2), (e) phase space of the variables (x_1, y_1, u).

i.e., they do not show quasiperiodic spiking. Below k_{SN}, where PRS undergoes its saddle node bifurcation SN_r, we can observe quasiperiodic spiking and at the critical coupling $k = \Delta$ both bursters adjust their frequencies and synchronize. As in Figure 10 this also influences the behavior

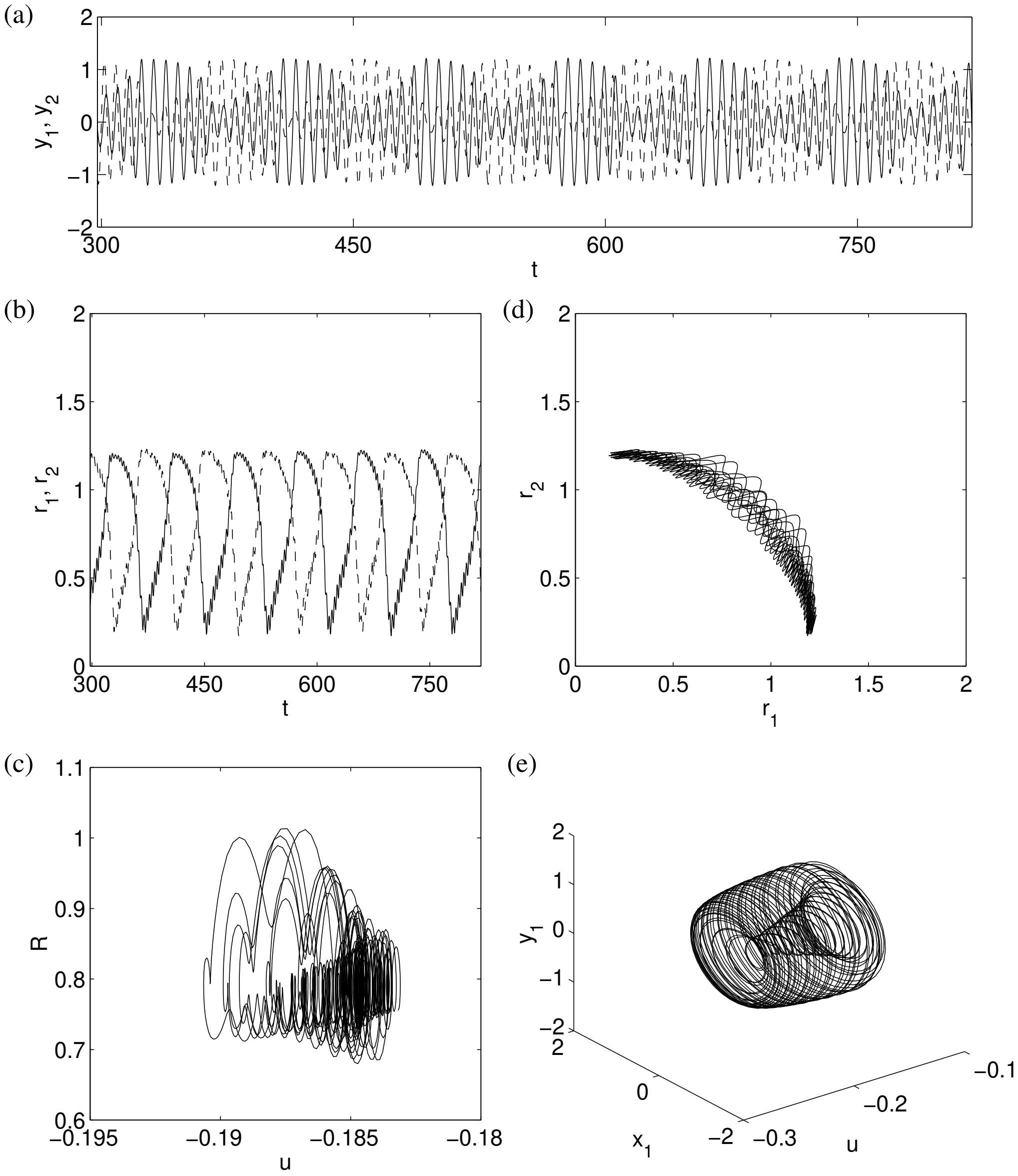

Figure 11: Two coupled elliptic bursters. Parameters as in Figure 6(a): $K = 0.04$, $\delta = 0.068$ ($\Omega_1 = 1$, $\Omega_2 = 0.7914$, $a = 0.79$, $b = 0.2$, $\mu = 0.005$, and $k = 0.16$). (a) Bursting patterns of the variables $y_i(t)$, (b) amplitudes r_i over time, (c) projection on (R, u), (d) projection on (r_1, r_2), (e) phase space of the variables (x_1, y_1, u).

of spike synchronization during a single burst. Both bursters may only "partially" synchronize. In the simulations both bursters perfectly synchronize their termination of bursting. The disability of perfect spike synchronization at onset of bursting may be explained by the slow passage effect.

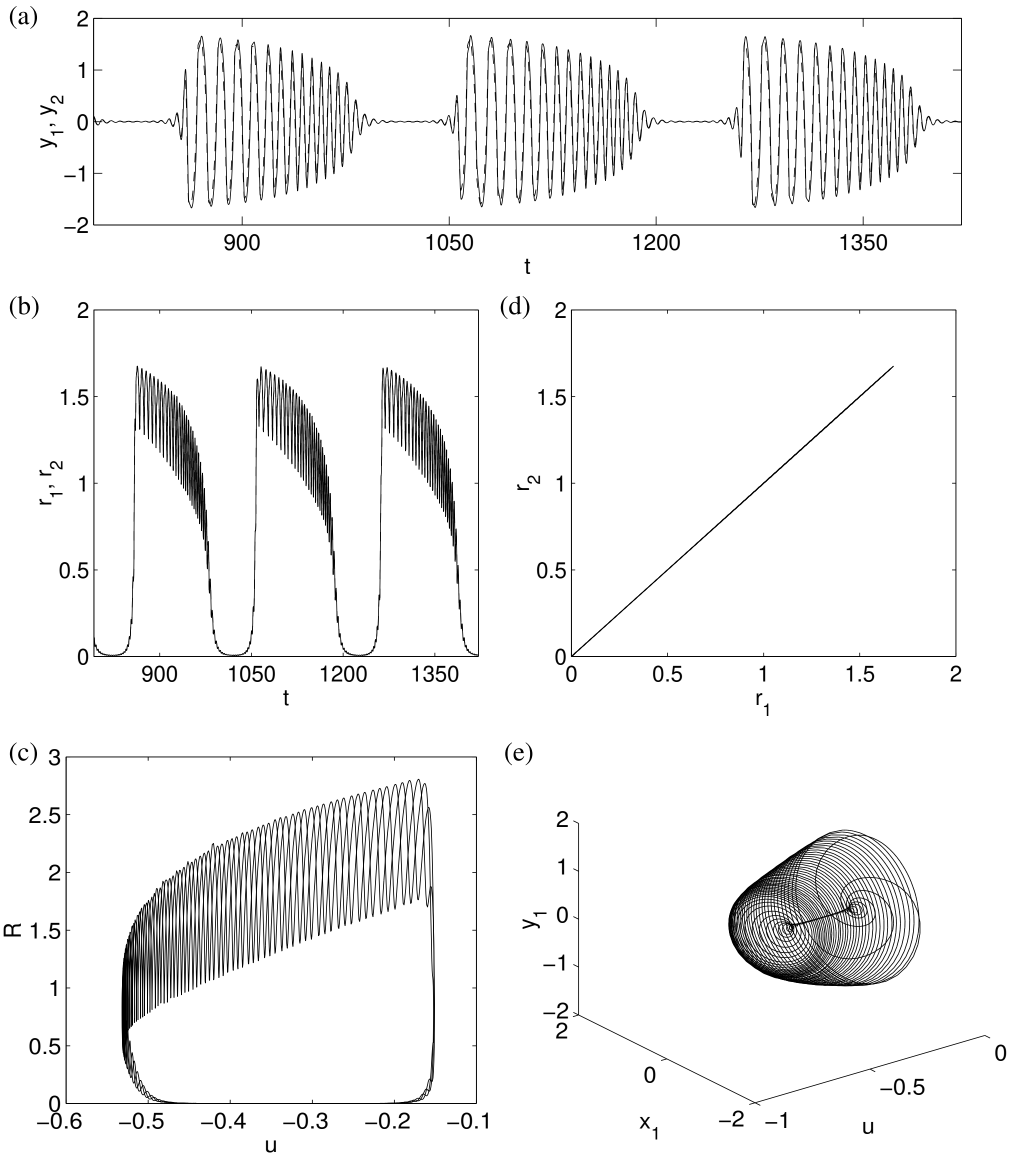

Figure 12: Two coupled elliptic bursters. Parameters as in Figure 6(d): $K = 0.075$, $\delta = 0.068$ ($\Omega_1 = 1$, $\Omega_2 = 0.7914$, $a = 0.79$, $b = 0.2$, $\mu = 0.005$, and $k = 0.692$). (a) Bursting patterns of the variables $y_i(t)$, (b) amplitudes r_i over time, (c) projection on (R, u), (d) projection on (r_1, r_2), (e) phase space of the variables (x_1, y_1, u).

Since both bursters do not influence each other significantly (which may also be indicated by the lack of small quasiperiodic amplitude oscillations near the steady state), the slow passage effect at onset of bursting is not affected by the other burster.

5 Discussion

In the present paper we investigated the effects of a small detuning of the spiking frequencies on the dynamics of two coupled elliptic bursters, i.e., bursters near subcritical Hopf bifurcation. Following the approach of Aronson et al. (1990) a reduced system of equations was derived. This simplifies the analysis substantially since for instance stable steady state solutions of the reduced system correspond to periodic solutions of the full system. The bifurcation structure of the reduced system was examined, revealing the influence of stationary and periodic bifurcations on the behavior of the full system. Aronson et al. (1990) carried out a detailed truncated normal form analysis for general, weakly nonlinear oscillators when the coupling strength is comparable to the strength of attraction to the limit cycle. However, this analysis deals with identical, non-relaxation oscillators near (stationary) supercritical Hopf bifurcations. de Vries et al. (1998) studied the interaction of a pair of weakly coupled biological bursters during the rapid oscillatory phase. Assuming that the uncoupled bursters are near a quasi-stationary supercritical Hopf bifurcation they extend the results of Aronson et al. (1990) to Hopf bifurcations with a slowly varying bifurcation parameter. Within their analyis they found a variety of oscillatory patterns of which asymmetrically phase-locked solutions are the most typical.

The main implication of the present bifurcation analysis for synchronization of coupled subcritical elliptic bursters is that a certain "overall" coupling constant must exceed a critical value depending on the detuning and the attraction rates in order that spike synchronization can take place. Our analytical and numerical results confirm the results of Izhikevich (2000a; 2000b) for identical elliptic bursters that burst synchronization is difficult to avoid and a dominat feature of elliptic bursters. In our analysis it can be found for small values of coupling strength. A frequency mismatch does not change this behavior significantly. Below the critical coupling the dynamics is characterized by burst synchronization and spike desynchronization, at least at onset of bursting. For identical oscillators our results are in good agreement with the theory of weakly connected neural oscillators near Hopf bifurcation developed by Hoppensteadt and Izhikevich (1997). Note that our analysis extended their results by an explicit formulation of synaptic coupling strength, detuning of the spike frequencies and the attraction rates of the oscillatory states during the active phase. We showed that oscillators with different frequencies can establish a common frequency of transmission as a result of increased synaptic coupling strength. In addition, changes in coupling strength can induce bifurcations which modify the firing patterns and the synchronization properties.

The results can easily be extended to other systems of oscillators, such as for example bistable van der Pol oscillators (Defontaines et al., 1990; Schwarz et al., 2000a). Although this analytical study is for two coupled bursters without external forcing, it can serve to explain some of the significant features observed in larger networks of bistable oscillators under external periodic stimulation (Schwarz et al., 2000a,b). There, modifying coupling strength and input frequency results in changes of the spatio-temporal patterns of the network and transitions between intrinsic and extrinsic dominated activity. For example, the occurrence of a saddle-node on limit cycle bifurcation for appropriate choices of frequency detuning and coupling strength in the network leads to a relaxation to the trivial fixed point in parts of the oscillators. When a periodic input is added, this is revealed as small amplitude (subthreshold) oscillation as was observed in our network simulations (Schwarz et al., 2000a,b)

The mechanisms of generation and modulation of biological rhythms and the nonlinear dynamics in interacting neural oscillators are of great importance in understanding the information processing abilities and functioning of biological neural systems. Neurons near Hopf bifurcation naturally incorporate the timing of neuronal firing as the phase of the oscillator and respond sensitively to the timing of incoming pulse trains. Class-2 excitability has been observed for example in stellate neurons of the entorhinal cortex (White et al., 1995) and elliptic bursting has been observed in rodent trigeminal interneurons (Del Negro et al., 1998). Many biophysical models of neuronal membrane dynamics also exhibit elliptic bursting, such as the FitzHugh-Rinzel, Chay-Cook, or Pernarowski models (Chay et al., 1995; Butera et al., 1995; Izhikevich, 2000a; de Vries and Miura, 1998; de Vries, 1998). An important source of control of the dynamical repertoire of a "real" neuron is neuromodulation (Butera et al., 1997; Guckenheimer et al., 1997; Fellous and Linster, 1997). Basically neuromodulation enhances or suppresses synaptic transmission by modifying intrinsic ion channel or synaptic properties. Altering coupling strength is thought as one way to represent neuromodulation. In our investigations different bursting behavior could be observed for nearby parameter values, i.e., small variations of synaptic coupling strength may change the neurocomputational properties of coupled bursters, i.e., determine the sensitivity upon input frequency and the ability to process incoming spike trains. In fact, biological systems may exploit this, e.g. for switching between different operating modes of neurons (Mukherjee and Kaplan, 1995). Since the observed behavior occurs close to the bifurcation point, i.e., for arbitrary small amplitudes, this may also be relevant for the generation of different subthreshold oscillatory patterns (White et al., 1995). Those patterns are essential for synchronization of neuronal ensembles since they impose periodic or chaotic fluctuations of the membrane potential close to threshold (Volgushev et al., 1998). Chaotic subthreshold oscillations may result in stochastic resonance (Lampl and Yarom, 1997; Longtin, 1997), i.e., they can enhance arbitrary weak incoming signals, and the possibility to lock these signals with the dominant frequency of the subthreshold oscillations.

References

D. Aronson, G. Ermentrout, and N. Kopell. Amplitude response of coupled oscillators. *Physica D*, 41:403–449, 1990.

S. Baer, T. Erneux, and J. Rinzel. The slow passage through a hopf bifurcation: delay, memory effects, and resonances. *SIAM J. Appl. Math.*, 49:55–71, 1989.

R. Bertram, M. Butte, T. Kiemel, and A. Sherman. Topological and phenomenological classification of bursting oscillations. *Bull. Math. Biol.*, 57:413–439, 1995.

P. Bressloff and S. Coombes. Desynchronization, mode locking, and bursting in strongly coupled integrate-and-fire oscillators. *Phys. Rev. Lett.*, 81:2168–2171, 1998.

R. Butera, J. Clark, and J. Byrne. Transient responses of a modeled bursting neuron: analysis with equilibrium and averaged nullclines. *Biol. Cybern.*, 77:307 – 302, 1997.

R. Butera, J. Clark, C. Canavier, D. Baxter, and J. Byrne. Analysis of the effects of modulatory agents on a modeled bursting neuron: dynamic interactions between voltage and calcium dependent systems. *J. Comput. Neurosci.*, 2:19 – 44, 1995.

T. Chay, Y. Fan, and Y. Lee. Bursting, spiking, chaos, fractals, and universality in biological rhythms. *Int. J. Bifurcation and Chaos*, 5:595 – 635, 1995.

G. de Vries. Multiple bifurcations in a polynomial model of bursting oscillations. *J. Nonlinear Sci.*, 8:281–316, 1998.

G. de Vries and R. Miura. Analysis of a class of models of bursting electrical activity in pancreatic β-cells. *SIAM J. Appl. Math.*, 58:607–635, 1998.

G. de Vries, A. Sherman, and H.-R. Zhu. Diffusively coupled bursters: effects of cell heterogenity. *Bull. Math. Biol.*, 60:1167–1200, 1998.

A. Defontaines, Y. Pomeau, and B. Rostand. Chain of coupled bistable oscillators. *Physica D*, 46: 201 – 216, 1990.

C. Del Negro, C.-F. Hsiao, S. Chandler, and A. Garfinkel. Evidence for a novel bursting mechanism in rodent trigeminal interneurons. *Biophys. J.*, 75:174–182, 1998.

G. Ermentrout. Type I membranes, phase resetting curves, and synchrony. *Neural Comput.*, 8: 979–1001, 1996.

J.-M. Fellous and C. Linster. Computational models of neuromodulation. *Neural Comput.*, 10: 771–805, 1997.

Z. Gil, B. Connors, and Y. Amitai. Differential regulation of neocortical synapses by neuromodulators and activity. *Neuron*, 19:679–686, 1997.

J. Guckenheimer, R. Harris-Warrick, J. Peck, and A. Willms. Bifurcations, bursting, and spike frequency adaption. *J. Comput. Neurosci.*, 4:257–277, 1997.

A. Hodgkin. The local electric changes associated with repetitive action in non-medulated axon. *J. Physiol.*, 107:165–181, 1948.

F. Hoppensteadt and E. Izhikevich. *Weakly connected neural networks.* Springer, 1997.

E. Izhikevich. Neural excitability, spiking, and bursting. *Int. J. Bifurcation and Chaos*, 10:1171–1266, 2000a.

E. Izhikevich. Subcritical elliptic bursting of Bautin type. *SIAM J. Appl. Math.*, 60:503–535, 2000b.

W. Kath. Resonance in periodically perturbed hopf bifurcations. *Studies in Appl. Math.*, 65: 95–112, 1981.

L. Lampl and Y. Yarom. Subthreshold oscillations and resonant behavior: two manifestations of the same mechanism. *Neurosci.*, 78:325–341, 1997.

H. Liljenström and M. Hasselmo. Cholinergic modulation of cortical oscillatory dynamics. *J. Neurophysiol.*, 74:288–297, 1995.

A. Longtin. Autonomous stochastic resonance in bursting neurons. *Phys. Rev. E*, 55:868–876, 1997.

P. Mukherjee and E. Kaplan. Dynamics of neurons in the cat lateral geniculate nucleus: In vivo electrophysiology and computational modeling. *Neurophysiol.*, 74:1222–1242, 1995.

T. Poston and I. Stewart. *Catastrophe Theory and its Applications.* Pitman, 1978.

J. Rinzel and Y. Lee. Dissection of a model for neuronal parabolic bursting. *J. Math. Biol.*, 25: 653–675, 1987.

J. Schwarz, K. Bräuer, G. Dangelmayr, and A. Stevens. Low-dimensional dynamics and bifurcations in oscillator networks via bi-orthogonal spectral decomposition. *J. Phys. A: Math. Gen.*, 33: 3555–3566, 2000a.

J. Schwarz, A. Sieck, G. Dangelmayr, and A. Stevens. Mode dynamics of interacting neural populations by bi-orthogonal spectral decomposition. *Biol. Cybern.*, 82:231–245, 2000b.

D. Somers and N. Kopell. Rapid synchronization through fast threshold modulation. *Biol. Cybern.*, 68:393 – 407, 1993.

M. Volgushev, M. Christiakova, and W. Singer. Modification of discharge patterns of neocortical neurons by induced oscillations of the membrane potential. *Neurosci.*, 83:15–25, 1998.

X.-J. Wang and J. Rinzel. Oscillatory and bursting properties of neurons. In M. Arbib, editor, *Brain Theory and Neural Networks*. MIT press, Cambridge, MA, 1995.

J. White, T. Budde, and A. Kay. A bifurcation analysis of neuronal subthreshold oscillations. *Biophys. J.*, 69:1203–1217, 1995.